GALAXY EVOLUTION IN GROUPS AND CLUSTERS

SATELLITE QUENCHING AND MORPHOLOGICAL TRANSFORMATION OF GALAXIES IN GROUPS AND CLUSTERS

By MEGAN OXLAND,

BSc. (University of British Columbia, Vancouver BC)

A Thesis Submitted to the School of Graduate Studies in Partial Fulfillment of the Requirements for the Degree Master of Science

McMaster University

MASTER OF SCIENCE (2023)

Hamilton, Ontario, Canada (Physics and Astronomy)

TITLE:	Satellite Quenching and Morphological Transformation of Galaxies in Groups and Clusters
AUTHOR:	Megan Oxland (McMaster University)
SUPERVISOR:	Dr. Laura Parker
NUMBER OF PAGES:	x, 88

Abstract

Galaxy properties are known to correlate with their environment, suggesting that environment plays a significant role in galaxy evolution. In particular, blue star forming spiral galaxies are preferentially found in low density regions while red, passive elliptical galaxies are found in the densest clusters. This suggests galaxies falling into groups and clusters experience a decrease in their star formation rate (SFR) and a morphological transformation from spiral to elliptical, but the timescales associated with these changes are not well constrained. This thesis explores the impact of environment on galaxy SFRs and morphologies for a large sample of galaxies from the Sloan Digital Sky Survey. We separate galaxies into two environments (groups and clusters) and use location in projected phase space as an estimate for how long a galaxy has been a part of its current environment. We calculate the timescales associated with the changes in galaxy SFRs and morphologies, and determine SFRs change more quickly than morphology. By comparing to a sample of field galaxies, we find evidence that prior group environments impact current galaxy properties via pre-processing.

Acknowledgements

One of the best decisions I have ever made was to complete my MSc here at McMaster University. Since my first day the Physics and Astronomy department has been a warm and welcoming environment, filled with people who have made my experience here a positive one.

Thank you to my friends (Taavishi, Jen, Blake, Mathew), office mates (Claude, Veronika, Jeremy, Kate), and members of my research group (Lauren, Dylan) for the many laughs and "little treats" along the way. To each and every one of you, know your future is bright and I look forward to future collaborations.

To my family and non-McMaster friends, thank you for your continued support throughout my many years of post-secondary. I know you are proud of me, and I know Mom would have been too.

Finally, I would like to thank my supervisor Dr. Laura Parker. Your patient nature and love of science made this experience truly amazing and I wouldn't change a thing. Your hike and restaurant suggestions were always appreciated, and I genuinely enjoyed learning from such an enthusiastic person. You are one of the most positive and supportive people I have ever met, so thank you for your guidance and encouragement over the past two years. I look forward to the next four!

Table of Contents

List of Figures

List of Tables

Co-Authorship

I, Megan Oxland, declare the contents of this thesis titled "Satellite Quenching and Morphological Transformation of Galaxies in Groups and Clusters" are my own and the work presented is original. Chapter 2 contains work submitted to the refereed journal *Monthly Notices of the Royal Astronomical Society* (MNRAS). I carried out all the data analysis, the preparation of the figures, and wrote the text of the paper. This work was co-authored with my supervisor, Dr. Laura Parker. The third and forth authors, R. R. de Carvalho and V. M. Sampaio, provided feedback on the manuscript before it was submitted. I hereby grant irrevocable, non-exclusive license to McMaster University and the National Library of Canada to reproduce the material as part of this thesis.

Chapter 1

Introduction and Motivation

Galaxies have fascinated astronomers for centuries, yet the study of galaxies began long before they were discovered to be separate stellar systems existing beyond the Milky Way. The first recorded observation of a galaxy was taken by Iranian astronomer Abd al-Rahman al-Sufi in the year 964, who described the Andromeda galaxy as a "small cloud" (Kepple & Sanner, 1998). For nearly eight centuries after this initial discovery, the study of galaxies continued yet remained largely qualitative. With the invention of telescopes, more distant objects could be observed resulting in catalogues of "nebulae" to be published in the late 18th century (Messier, 1774; Herschel, 1786). At this point in time, any celestial object that were not a comet and appeared fuzzy were referred to as nebulae.

In the late 19th century, photography began to revolutionize the field and allowed astronomers to study the structure of nebulae in detail. Hubble (1925) discovered several Cepheid variable stars in the Andromeda nebula, resulting in a distance measurement using the Cepheid period-luminosity relation (Leavitt & Pickering, 1912).

This distance provided conclusive evidence that M31 was an extragalactic object completely separate from the Milky Way (Hubble, 1925). This paved the way for the next 100 years of galaxy science.

The study of galaxies has been revolutionized in modern times with deep and wide surveys of the extragalactic sky such as the Sloan Digital Sky Survey (SDSS; York et al. (2000)), the Cosmic Evolution Survey (COSMOS; Scoville et al. (2007)), the Galaxy and Mass Assembly survey (GAMA; Driver et al. (2011)), and the Dark Energy Survey (DES; Abbott et al. (2018)) to name a few. With measurements of millions of galaxies at varying distances, we are now able to carry out extensive statistical studies of how galaxy properties evolve over cosmic time.

1.1 Galaxy Properties

Galaxies are complex dynamical systems that contain stars, gas, and dust located within an extended dark matter halo. There are a wide range of physical properties associated with galaxies, so understanding how these change over cosmic time is key to understand galaxy evolution. In this section, I will outline some of the key properties used when studying galaxies, including their morphology, mass, colour, and star formation rate.

1.1.1 Morphology

The first morphological classification scheme was created by Edwin Hubble in 1926, and separates galaxies based on their visual morphology (Hubble, 1926). Known colloquially as Hubble's tuning fork diagram (see Fig. 1.1), this system broadly

separates galaxies as either elliptical, spiral, or irregular. Elliptical galaxies are further subdivided into eight classes based on ellipticity (e=0,1,...,7), where $e = 10 \times (a - b)/a$ with a and b representing the projected major and minor axes of the ellipse, respectively. Ellitpicals are then labeled E0, E1, ..., E7, with E0 referring to a perfect circle and E7 being a highly elongated ellipse. Spiral galaxies are sub-divided based on structural features, namely whether they have a central bar, the size and brightness of the central bulge, and how tightly coiled the spiral arms are. Sa galaxies are those with bright central bulges and tightly wound spiral arms, while Sc galaxies are those with looser arms and a smaller bulge. Sb galaxies are an intermediate population. SBa, SBb, and SBc are analogous classifications, but for galaxies hosting central bars. An additional third class of lenticular (S0) galaxies was later added to bridge the gap between ellipticals and spirals (Hubble, 1936). These galaxies have bulges and limited disks but no spiral arms.

Elliptical/S0's and spiral galaxies are commonly referred to as "early-types" and "late-types", respectively. It should be noted this nomenclature is purely descriptive and does not describe an evolutionary pathway. Also, when using this visual classification system a number is often assigned to galaxies of different classes called the T-Type parameter (de Vaucouleurs, 1963). Early-type galaxies are classified by T-Type ≤ 0, while late-types have T-Type > 0.

This visual classification system was the primary way astronomers separated galaxies for decades, imaging individual galaxies and manually classifying each one by eye. This worked for catalogues of a couple thousand galaxies (Fukugita et al., 2007; Nair & Abraham, 2010) but with the explosion of large surveys it quickly became too time consuming and no longer feasible. Astronomers instead turned to three

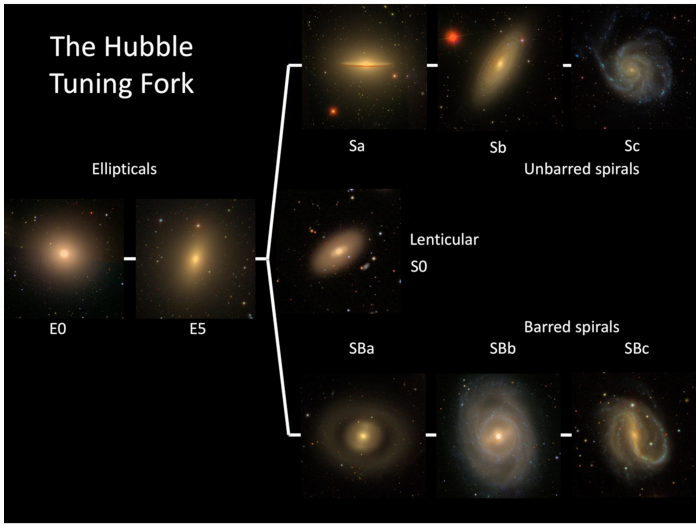

Figure 1.1: Galaxy morphology based on the Hubble tuning fork diagram. Elliptical galaxies are on the left, spiral galaxies are on the right (Masters et al., 2019, Figure 1).

main methods to classify galaxy morphology: citizen science, machine learning, and quantitative metrics.

Citizen science projects use members of the public to classify galaxies based on images. The pioneering project was Galaxy Zoo, a web-based platform that classified $\sim 9 \times 10^5$ SDSS galaxies (Lintott et al., 2008, 2011b). Galaxy Zoo 2, a follow-up project, improved upon its predecessor by including finer morphological features such as bars, bulges, disks, mergers, and the strength of spiral arms (Willett et al., 2013). These citizen science catalogues are then used as training sets for machine learning deep learning algorithms to calculate galaxy morphology (Domínguez Sánchez et al., 2018; Huertas-Company et al., 2011). Quantitative morphology metrics use direct measurements from surface brightness profiles, which can be easily applied to large galaxy imaging surveys. In the following subsections, I briefly explain two common

morphology measures calculated from photometry including Sérsic indices and bulge-to-total ratios.

Sérsic Index

The Sérsic index (n) is the free parameter of the Sérsic profile (Sérsic, 1963; Sersic, 1968) which describes a galaxy's radial light profile. It is defined by

$$I(R) = I_e \exp\left\{-b_n\left[\left(\frac{R}{R_e}\right)^{1/n} - 1\right]\right\} \tag{1.1.1}$$

where I_e is the intensity at the effective radius R_e, and b_n is a function of n (Caon et al., 1993). In practice Sérsic indices can range anywhere from $0.5 \leq n \leq 10$. Spiral galaxies are well fit by small Sérsic indices ($n \leq 2$), with pure disk galaxies following exponential profiles ($n = 1$). Elliptical galaxies are well fit by larger Sérsic indices ($n \geq 2$), with the de Vaucouleurs profile ($n = 4$) a common choice for early-type galaxies (de Vaucouleurs, 1948). Sérsic profiles cannot capture distinct features such as spiral arms or bright clumps, but provide good models for the smooth component of galaxy light.

Bulge-to-Total Ratio

Instead of modeling an entire galaxy with one Sérsic profile, bulge+disk decompositions can be used to classify galaxy morphology. The light profile of the bulge and disk components are fit separately, often by a $n = 4$ bulge and $n = 1$ disk. The separate profiles can then be combined into one measure of morphology, the bulge-to-total ratio (B/T). B/T is defined as the fraction of the total flux contained in the bulge component of a galaxy compared to the total flux. This measurement provides

a continuous number between 0 and 1, ranging from completely disk dominated with no bulge component (B/T=0) to completely bulge dominated (B/T=1). Today, these two-component fits are often done through open-source codes such as GALFIT (Peng et al., 2002, 2010a) and GIM2D (Simard et al., 2002, 2011).

1.1.2 Mass

Galaxy mass is a notoriously difficult property to measure. One popular method for measuring the total mass of a galaxy is to measure the rotation speed of stars or gas as a function of radius from the galaxy centre. Then the mass contained within a given radius can be estimated through $M(R) = v^2R/G$ (equating the centripetal force and the force of gravity). Rubin & Ford (1970) studied the rotation curve of M31 and discovered that at large radii the curve flattened instead of decreasing as expected. This flat rotation curve is common for spiral galaxies (Rubin et al., 1980), and suggests that galaxy mass is dominated by dark matter. Measuring the total mass, dominated by dark matter, via kinematic or dynamical measurements is challenging and requires extensive spectroscopy. Instead of total mass, astronomers often look at galaxy stellar mass (M_*).

Stellar mass is the total mass of a galaxy contained in stars. Today, the most common way of estimating M_* is through spectral energy distribution (SED) fitting. An SED measures the energy emitted by an object as a function of wavelength. Since different wavelengths correspond to the emission coming from different sources (see Fig. 1.2), a wealth of information can be extracted from one SED. To calculate stellar mass, many stellar population synthesis (SPS) models are stacked to create a synthetic spectrum (Tinsley, 1980; Vazdekis, 1999; Bruzual & Charlot, 2003). This is

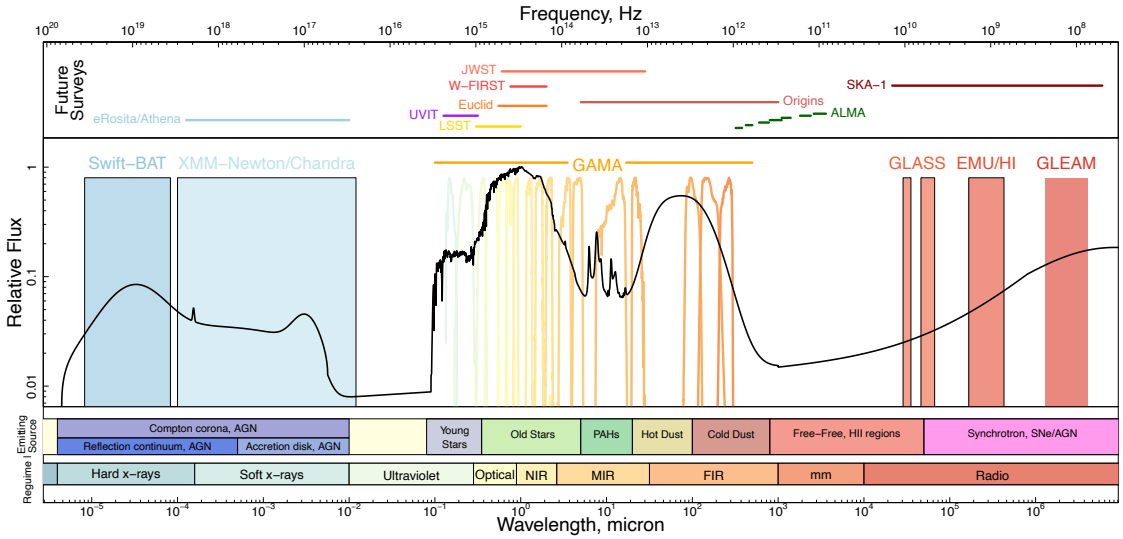

Figure 1.2: An example galaxy spectral energy distribution (SED) shown in black. The top panel shows the wavelength coverage of recent and future surveys. The bottom panel shows the physical processes that emit in different wavelength regimes. Coloured regions behind the SED show the broadband filter coverage of various surveys (Figure by Dr. Luke Davies, reproduced here with permission).

then compared to the true galaxy SED, and the best fit model provides an estimate of M_*, as well as star formation histories, star formation rates, ages, etc.

Although there are a number of popular SED fitting codes available (e.g. `ProSpect` Robotham et al. (2020), `Bagpipes` Carnall et al. (2018), `CIGALE` Boquien et al. (2019)), they all make different prior assumptions and therefore can vary from one another. Choices must be made on the initial mass function (IMF) and the behaviour of metallicity, dust emission, AGN, and stars (Thorne et al., 2021). To complicate things further, one rarely has access to the entire SED and modelling must be done for only a small wavelength range.

In the past few decades, stellar mass has been shown to correlate with various galaxy properties. For example, star formation rates (see Sec. 1.1.4), size, central black hole mass, and quenched fractions all increase with increasing M_* (Brinchmann

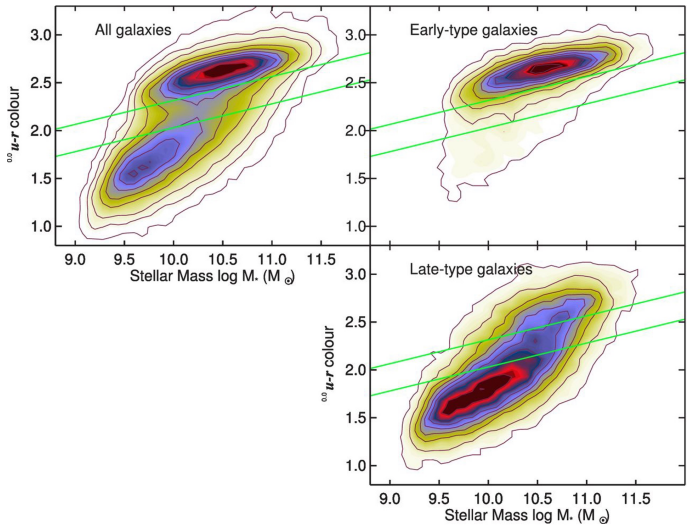

Figure 1.3: Galaxy u-r colour versus mass diagram for a selection of SDSS galaxies (Schawinski et al., 2014, Figure 2). The total sample is shown in the top left, which is then split by morphology into early-type (top right) and late-type galaxies (bottom right). Early-type galaxies populate the "red sequence", late-type galaxies populate the "blue cloud". The "green valley" divides the two distinction populations and is shown by the region bounded by the diagonal green lines.

et al., 2004; Shen et al., 2003; Reines & Volonteri, 2015; Wetzel et al., 2012). There is also the stellar-to-halo mass relation, where there is a tight relationship between the stellar mass of a galaxy and the dark matter halo in which it resides (e.g. Wechsler & Tinker, 2018). Many of these properties also vary with redshift, but typical galaxy stellar masses in the local universe range from $10^9 - 10^{11.5} M_\odot$, with galaxies lower than $10^9 M_\odot$ referred to as dwarf galaxies (Carroll & Ostlie, 2017).

1.1.3 Colour

Colour is defined as the difference in magnitude of a galaxy in two different broadband photometric filters. These filters are sensitive to specific wavelengths of light and therefore only allow light of a specific frequency range to pass through. The SDSS

has five standard filters labeled u, g, r, i, z with median wavelengths corresponding to 3550Å, 4770Å, 6230Å, 7620Å, and 9130Å, respectively (Gunn et al., 1998; Abazajian et al., 2003). The commonly used optical colour u-r for example is the difference in galaxy flux measured in the ultraviolet filter (u) and the red filter (r). Since magnitudes are smaller for brighter objects, small u-r colours are more blue compared to large u-r colours which are more red.

Galaxy colour is found to be bimodal when looking at the distribution of one colour for a large sample of galaxies (e.g. a u-r histogram is well fit by two gaussians; Strateva et al., 2001). This colour bi-modality was also found to extend to galaxy morphology, where early-type galaxies are more red while late-type galaxies are more blue (de Vaucouleurs, 1961). This colour bi-modality and correlation with morphology has since been extended to more distant surveys, where the colour of galaxies has been found to be bimodal out to at least z$\sim$1 (Baldry et al., 2004b; Bell et al., 2004). Colour-mass diagrams clearly show two distinct populations (Fig. 1.3), where early-types populate the red sequence and late types populate the blue cloud. The green valley is a transition region and separates the two populations (Salim, 2014).

Galaxy colours also depend strongly on stellar mass, where the red sequence extends to higher masses compared to the blue cloud. This result has been supported by several works which have found the fraction of red sequence galaxies and the colour of galaxies both increase with stellar mass (e.g Baldry et al., 2006; van den Bosch et al., 2008; Prescott et al., 2011). Although colour is a relatively easy property to measure, the effects of dust and redshift on colour must be accounted for.

1.1.4 Star Formation Rate

Star formation is a complex process that begins with the collapse of a large, cold, dense giant molecular cloud. The star formation rate (SFR) of a galaxy is defined as the mass of stars formed per year, typically measured in $M_\odot$/yr. Since star formation is influenced by both internal and environmental processes (see Sec. 1.3), being able to accurately measure SFRs is crucial when studying galaxy evolution. There are a number of ways astronomers determine SFRs; here I present a brief overview of some of the most common measures of SFR. I refer the reader to Kennicutt (1998) and Kennicutt & Evans (2012) for a more detailed discussion of other SFR measures.

UV and IR Continuum Emission

Some SFR indicators measure galaxy star formation by directly measuring the emission from the underlying stellar population. Since young, hot stars emit primarily in the UV, UV continuum emission probes the light coming from newly formed stars. As a result, this diagnostic is one of the best tracers of recent star formation over the past 10-200 Myr (Kennicutt & Evans, 2012). This method of determining SFRs was revolutionized by the launch of the GALEX spacecraft (Martin et al., 2005), which provided SFRs for hundreds of thousands of galaxies in the redshift range $0 < z < 2$.

One major disadvantage of measuring SFRs with UV luminosities is the effect of interstellar dust, which strongly absorbs UV photons and re-emits them in the IR. Using IR continuum emission to trace this obscured star formation has proven to be a useful way to measure SFRs, especially in dusty galaxies. With the launch of IR telescopes such as the Spitzer Space Telescope (Werner et al., 2004) and the Wide-field Infrared Survey Explorer (WISE; Wright et al., 2010), IR SFRs could now

be measured. Today, UV and IR observations are often combined to measure dust-corrected SFRs (Kennicutt & Evans, 2012), improving the SFRs measured from UV or IR individually.

Hα Emission and Other Recombination Lines

Young massive stars emit strong radiation that is able to ionize the surrounding gas in the interstellar medium (Boissier, 2013). The recombination lines that are produced from this ionization can then be used as a SFR indicator. The most commonly used recombination line at low redshifts is Hα, the first line in the Hydrogen Balmer series detected at an optical wavelength of 6563Å (Moustakas et al., 2006). This is one of the most instantaneous measures of SFR, tracing stars with lifetimes of 3-10 Myr (Kennicutt & Evans, 2012). At intermediate redshifts where Hα is shifted into the IR ($z \geq 0.4$), the [OII] emission line can be used instead (Kennicutt, 1992). At even higher redshifts, the Lyα recombination line can be used (Kennicutt & Evans, 2012).

Recombination lines are sensitive to dust and therefore require extinction corrections often estimated from line ratios. For Hα, the ratio Hα/Hβ called the "Balmer decrement" is often used to measure the amount of flux obscured from dust and therefore corrects the corresponding Hα SFR (Boissier, 2013).

D4000

Another commonly used SFR indicator is D4000, which is a measure of the break strength of a galaxy spectrum at 4000Å. First introduced by Hamilton (1985), the modern definition of D4000 was revised by Balogh et al. (1999) to be the ratio of flux in the red continuum (4000-4100Å) to that in the blue continuum (3850-3950Å).

D4000 traces star formation on long timescales and is a measure of the age of the stellar population in a galaxy. Large D4000 indices are measured in old galaxies with no recent star formation (Balogh et al., 1999), while galaxies that are actively forming stars have small D4000 breaks.

SED Fitting

The emission from galaxies emitted at different wavelengths can be combined together to determine SFRs through SED fitting. Similar to how astronomers measure galaxy mass (see Section 1.1.2), SED fitting assumes galaxy spectra are the product of the emission from individual galaxy components (i.e. ISM, stars, AGN, etc.) stacked on top of one another. Making many prior assumptions such as an IMF, stellar spectra templates, metallicities, dust distributions etc., model spectra can be compared to the actual galaxy spectrum (Walcher et al., 2011). The best fit model SED provides estimates for the stellar mass, SFR, ages, and star formation histories of galaxies.

The Star Forming Main Sequence

When SFR is plotted against stellar mass, yet another bimodality appears (see Figure 1.4). The population with higher star formation rates has a linear relationship in log space with stellar mass and lies along the so called "star forming main sequence" (SFMS; Noeske et al., 2007). However, the actual shape of this line is debated and thought to become flatter at the high mass end (e.g. Tomczak et al., 2016; Popesso et al., 2019). Nonetheless, the slope of the main sequence is known to depend on the SFR indicator used (Popesso et al., 2019), and it is dependent on redshift where the SFMS is shifted vertically up toward higher SFRs at higher redshifts (e.g. Speagle

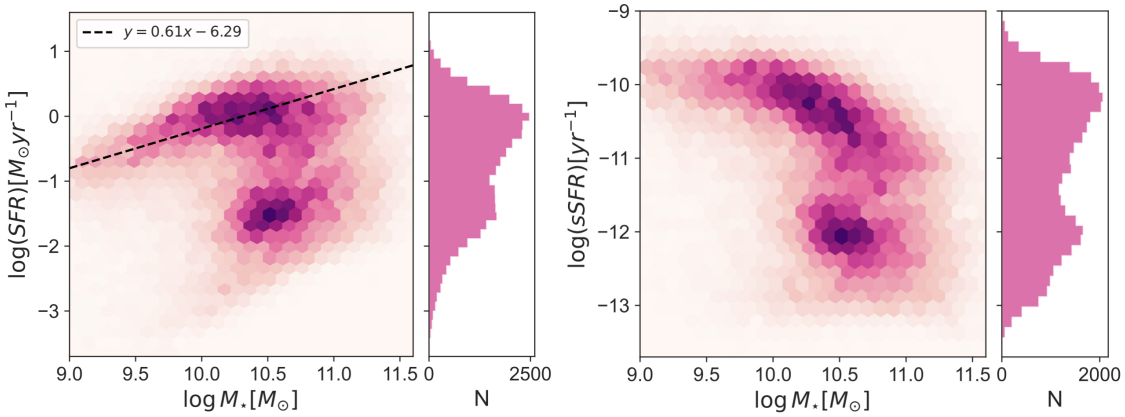

Figure 1.4: Left: Galaxy SFR as a function of stellar mass for a selection of SDSS galaxies in my sample. SFRs were measured via SED fitting. The black dashed line corresponds to the star forming main sequence and was determined by fitting a straight line to all galaxies with $\log_{10}(\text{sSFR}) < -11[\text{yr}^{-1}]$. Right: The sSFR as a function of stellar mass for the same sample. The bimodality in both SFR and sSFR can be seen in the vertical histograms to the right of each plot.

et al., 2014; Popesso et al., 2023). This suggests galaxies are less star forming today than they were in the past, supported by other studies which have found the average SFR density peaked at $z \sim 2$ (e.g. Madau et al., 1998; Hopkins & Beacom, 2006). Starburst galaxies are those that lie above the SFMS.

Since SFR has a dependence on stellar mass, astronomers often normalize SFR by mass and study specific star formation rate (sSFR=SFR/$M_\star$). sSFR as a function of stellar mass is shown in Figure 1.4, where two populations again emerge separated at $\log(\text{sSFR}) \sim -11[\text{yr}^{-1}]$. This dividing line in the sSFR-M_* plane separates galaxies actively forming stars (above) from those that are passively evolving (below). The persistent bimodality in morphology, colour and SFR/sSFR in general all coincide with each other. This indicates there are two main populations of galaxies: (1) blue, late-type galaxies that are actively forming stars and (2) red, early-type galaxies with little to no star formation. This bimodality has led to the general consensus that

galaxies start out in the blue cloud where they lie on or near the SFMS, experience a decrease in SFR which moves them off the SFMS into the green valley, and finally they move into the red sequence once star formation has been halted. The process by which galaxy star formation stops is referred to as "quenching", yet a small subset of galaxies experience "rejuvenation" where star formation starts up again after being quenched (Rampazzo et al., 2007). This thesis is primary interested in tracing galaxies as they quench, and understanding the different mechanisms (see Section 1.3) that drive this evolution through different environments.

1.2 Galaxy Environments

Throughout the universe galaxies are found to exist in a wide range of environments. They can either be isolated as field galaxies, or in gravitationally bound systems of galaxy groups or rich galaxy clusters. These dense environments are dynamically complex and can contain thousands of galaxies all orbiting around their common centre of mass. Being able to measure and understand the particular environment in which a galaxy resides is critical to gain a complete picture of galaxy evolution.

1.2.1 Field

Field galaxies are those found isolated in the universe that have not experienced any recent perturbations from neighbouring galaxies. They are the best available laboratories for astronomers to study the secular processes by which galaxies evolve, including feedback from stars and active galactic nuclei (see Section 1.3.1). The first catalogue of 1050 isolated galaxies was published by Karachentseva (1973) and were

Figure 1.5: Left: An image of Robert's Quartet taken with the VLT. It is a compact group with four member galaxies at a distance of 49 Mpc (Image credit: ESO). Right: The Coma Cluster, a nearby cluster of > 1000 galaxies 99 Mpc from Earth (Image credit: NASA, ESA, Hubble Heritage Team).

identified by pure 2D visual inspection. With the advent of large surveys able to measure spectroscopic redshifts (e.g. SDSS), the classification of field galaxies has since improved leading to larger and more robust catalogues (e.g. Argudo-Fernández et al., 2015).

Blue galaxies with spiral morphologies are dominant in the field, yet isolated early-type galaxies (iETG) do exist (Dressler, 1980; Goto et al., 2003). These iETGs are of interest to astronomers since many show signatures of rings, tails, and shells thought to be due to interactions and mergers (Reduzzi et al., 1996; Rampazzo et al., 2020). Field galaxies have also been found to have similar properties to high redshift galaxies, supporting the idea that the field galaxies in the local universe are the "unused building blocks" that have not yet formed into groups and clusters (Varela et al., 2004). On average, field galaxies have higher star formation rates and younger mean stellar populations than those in denser environments (de Carvalho & Djorgovski,

1992; Blanton & Moustakas, 2009).

1.2.2 Galaxy Groups and Clusters

Most galaxies in the universe are found in gravitationally bound groups or clusters, where the mass is dominated by the dark matter halo in which they reside (Carroll & Ostlie, 2017). Galaxy groups are the most common environment and they contain no more than ∼50 members (Eke et al., 2005; Carroll & Ostlie, 2017). There is no universal definition, yet in general most galaxy groups satisfy (Mamon, 2007):

- Total halo masses of $10^{13} \leq \mathrm{M}_{200} \leq 10^{14}\mathrm{M}_{\odot}$
- Virial radii of $0.3 \leq \mathrm{r}_{200} \leq 1\mathrm{Mpc}$
- Velocity dispersions of $140 \leq \sigma_v \leq 450\mathrm{kms}^{-1}$

An example of a famous group is Robert's Quartet shown in Figure 1.5. This group has four member galaxies all with different morphologies. Since groups have low velocity dispersions, many show signs of previous interactions such as high asymmetries and tidal tails (e.g Toomre & Toomre, 1972; Hernández-Toledo et al., 2006; Mamon, 2007).

Galaxy clusters can contain anywhere from 50 galaxies in a poor cluster, to thousands of galaxies in a rich cluster (Carroll & Ostlie, 2017). The central brightest (and often most massive) galaxy is called the 'central', while all other members are referred to as satellites. Clusters are permeated by hot plasma called the Intracluster Medium (ICM), which emits radiation at X-ray wavelengths. The ICM has temperatures of $10^7 - 10^8 K$, and is composed primarily of ionized hydrogen and helium (Molendi, 2004). Although the ICM is not very dense (usually between $10^{-4} - 10^{-2}\mathrm{cm}^{-3}$), it

can have an influence on galaxies as they fall into clusters (see Section 1.3). There is no universal definition of a cluster, but they have higher masses, larger virial radii and higher velocity dispersions compared to the values listed above for groups. Clusters typically have $M_{halo} \geq 10^{14} M_{\odot}$ (Carroll & Ostlie, 2017).

Although there are several ways environment can be measured, they all correlate well with local overdensity and show trends with various galaxy properties. Perhaps the most well known is the morphology-density relation of Dressler (1980), which found low density environments are dominated by spiral galaxies and high density environments are dominated by ellipticals. Clear environmental trends can also be seen in individual clusters, where the centrals are often large, red elliptical galaxies residing at the centre of the potential well. An example of a rich cluster is the Coma Cluster shown in Figure 1.5. This nearby cluster has over 1000 galaxies of varying morphologies, yet the centre is clearly dominated by ellipticals.

In addition to morphology, several other galaxy properties have been found to depend on environment including SFR (e.g. Balogh et al., 1998; Hashimoto et al., 1998; Tanaka et al., 2004; Wetzel et al., 2012) and colour (e.g. Baldry et al., 2006; Bamford et al., 2009; Masters et al., 2010). Group and cluster galaxies in general are redder and have lower SFRs than field galaxies. This is true in individual clusters as well, where galaxies near the centre are redder, have early type morphologies and are less star forming than those at large cluster-centric radii (e.g. Postman et al., 2005; Park & Hwang, 2009; Fasano et al., 2015).

Identifying groups and clusters in large observational surveys and simulations is often done through group-finding algorithms. These take into account projected distances between galaxies, their line of sight velocities, and their redshifts to identify

galaxies that are likely gravitationally bound to each other. A commonly employed algorithm is friends-of-friends (FOF), which takes a linking length and connects galaxies within that angular distance (Huchra & Geller, 1982; Press & Davis, 1982). This is performed iteratively on group members until there are no changes in group membership. The SDSS group catalogue of Yang et al. (2007) uses an improved halo-based group finder which uses luminosity to estimate the halo mass, size, and velocity dispersion of the group. These are then used to assign galaxies to specific halos, after the group centres are found using the traditional FoF algorithm. This method has the advantage of being able to identify field galaxies, and is the group catalogue used in this thesis.

1.3 Galaxy Quenching Mechanisms

Galaxies are dynamic systems which are constantly undergoing evolutionary changes including a number of possible quenching mechanisms. These processes have an effect on the cold gas component of a galaxy, and suppress star formation and change galaxy morphology as a result. Quenching mechanisms can broadly be separated into internal and environmental mechanisms, some of which are described in the subsections below.

It is important to point out that structure growth in the universe is a hierarchical process where field galaxies combine to form groups, which then merge together to form galaxy clusters. As a consequence, galaxies in clusters may have experienced pre-processing in which they have been affected by their previous environment (e.g. Fujita, 2004; Wetzel et al., 2013). This complicates the understanding of galaxy evolution as it is difficult to disentangle the effects of a prior group from the current cluster.

1.3.1 Internal Processes

Internal mechanisms are processes that affect all galaxies no matter the environment in which they reside. These processes include both injection of energy and matter back into the ISM through feedback, and the stellar bulge stabilizing molecular clouds in the disk against collapse via morphological quenching (Walch et al., 2012; Fabian, 2012; Martig et al., 2009).

Stellar Feedback

Important for most galaxies, especially those with late-type morphologies, is stellar feedback; the injection of energy, momentum and mass back into the ISM through the evolution of stars. Initially, this feedback is driven by ionizing radiation and stellar winds from young, massive stars which greatly influences the future evolution of molecular clouds (Walch et al., 2012). The outward pressure arising from radiation and wind often is strong enough to expand surrounding HII regions, creating voids around newly formed stars (Tenorio-Tagle & Bodenheimer, 1988). This process can either trigger new star formation at the edge of these bubbles (Elmegreen & Lada, 1977; Elmegreen, 1998), or terminate star formation due to the disruption of molecular clouds (Tenorio Tagle et al., 1979; Williams & McKee, 1997; Matzner, 2002). Bubbles created from stellar feedback can be seen in Figure 1.6.

Massive stars end their lives as supernovae which can inject vast amounts of energy and momentum into the surrounding ISM, forming large superbubble structures (e.g. McKee & Ostriker, 1977; Keller et al., 2014). This force can be so great that material can be blown out of the galactic disk, depositing hot gas into the halo (Tomisaka & Ikeuchi, 1986; Fraternali, 2017; Keller et al., 2020).

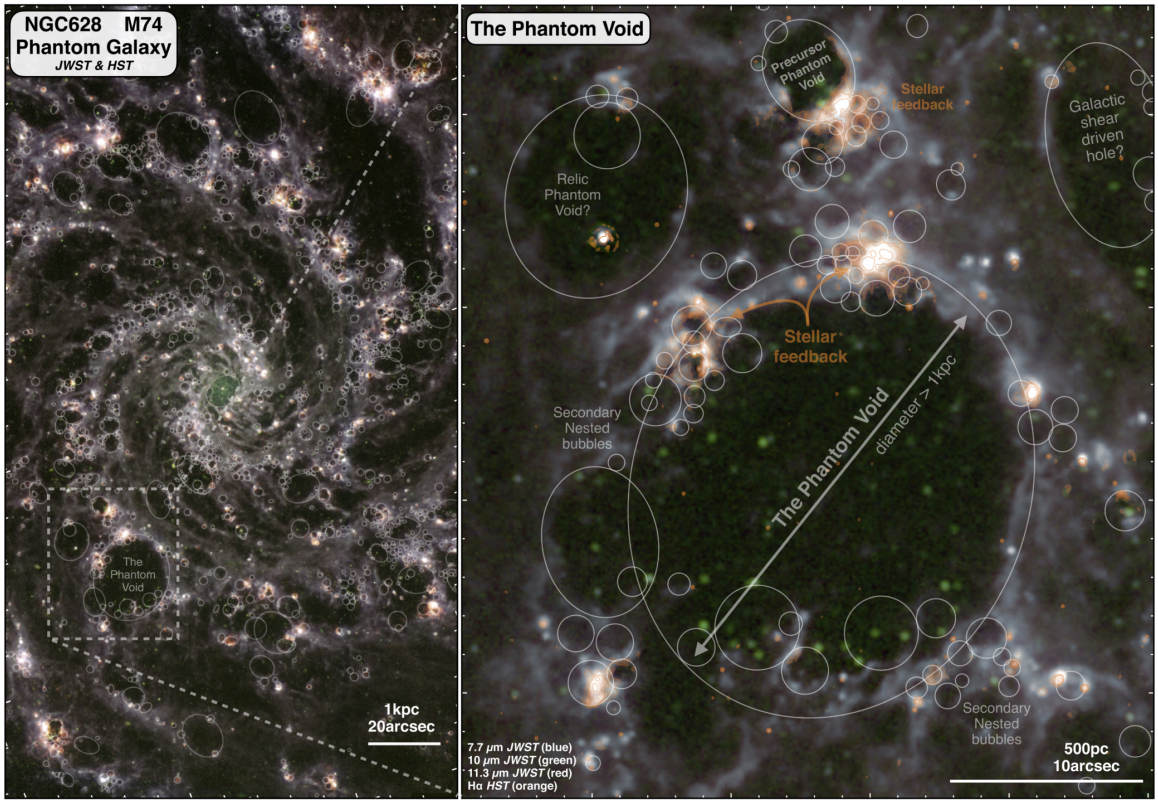

Figure 1.6: Composite image of the Phantom Galaxy (NGC 628) produced from the 770W (blue), 1000W (green), and 1130W (red) filters from the JWST. Orange shows recent star formation as traced by Hα emission from the HST. The grey ellipses show the locations of identified bubble structures (Barnes et al., 2023, Figure 1)

AGN Feedback

Supermassive black holes reside at the the centres of most galaxies, and when they accrete material from the surrounding ISM they are referred to as active galactic nuclei (AGN). AGN release energy in the form of radiation, winds, and jets that can both prevent surrounding gas from cooling, and remove central cold gas via outflows (see review by Fabian, 2012). In galaxy simulations, AGN prescriptions have proved necessary to reproduce observations of quenched massive galaxies (Bower et al., 2006; Gabor et al., 2011; Somerville & Davé, 2015; Su et al., 2019).

Morphological Quenching

Star formation takes place primarily in the disks of late-type galaxies, when giant molecular clouds (GMCs) fragment and collapse. If something were to stabilize the disk against fragmentation, GMCs will not collapse and star formation will subsequently quench. This is referred to as morphological quenching, and is often attributed to the growth of the stellar bulge (Martig et al., 2009). Through simulations this spheroidal component has shown to increase the central gas velocity dispersion, which stabilizes the gas disk and suppresses star formation (e.g. Martig et al., 2013; Gensior et al., 2020). However, there must be some additional mechanism to trigger the growth of the bulge such as major and minor mergers (Brooks & Christensen, 2016), or the existence of a bar to drive material into the central regions (Kormendy & Kennicutt, 2004)

1.3.2 Environmental Mechanisms

Environmental mechanisms are all the processes that impact the SFR and morphology of a galaxy due to their environment. Most galaxies are found in groups and clusters where star formation is known to be suppressed (e.g. Balogh et al., 1998; Wetzel et al., 2012). It is therefore necessary to understand the various mechanisms acting on these galaxies and how they change galaxy properties over cosmic time.

Ram Pressure Stripping

As galaxies plow through the hot ICM that exists between cluster satellite galaxies, they can be affected by ram pressure (e.g. Gunn & Gott, 1972; Fujita, 2001). This pressure is given by $P = \rho_{ICM} v_{rel}^2$, where ρ_{ICM} is the ICM density and v_{rel} is the relative velocity between the galaxy and the ICM (Gunn & Gott, 1972). If the ram pressure is strong enough, the cold gas from the galactic disk can be removed via ram pressure stripping (RPS). This is a quenching mechanism effective in the most massive environments, where ICM densities and relative velocities are high (Abadi et al., 1999; Boselli et al., 2022),

RPS signatures often include long tails of stripped material trailing behind infalling galaxies (see Figure 1.7; Chung et al., 2007; Poggianti et al., 2017), and the outer edges of galactic disks being truncated leading to outside-in quenching (Quilis et al., 2000; Sun et al., 2007; Chung et al., 2007). The most extreme RPS galaxies are refereed to as "Jellyfish" galaxies due to their peculiar morphologies and long tentacles of stripped material (Smith et al., 2010b). Even though RPS is commonly considered a quenching mechanism, star formation has been observed in the stripped ISM (e.g. Cortese et al., 2007; Hester et al., 2010; Vulcani et al., 2018). There is also

Figure 1.7: Composite image of ESO 137-001, a ram pressure stripped galaxy in the Norma Cluster (Abell 3617) moving toward the top left. The image was taken by HST, with X-ray light from the Chandra X-ray Observatory in blue revealing a tail of stripped gas (Image credit: NASA, ESA, CXC).

evidence that the compression of the ISM due to ram pressure upon initial infall can trigger an episode of enhanced star formation on the leading side of a galaxy (Roberts & Parker, 2020; Troncoso-Iribarren et al., 2020; Roberts et al., 2022).

Strangulation & Starvation

While RPS affects the cold ISM in the galactic disk, other processes affect the hot gas contained in the surrounding halo. Strangulation is a quenching mechanism by which only the hot halo of a galaxy is stripped away upon infall (Larson et al., 1980). This removes the gas that would have otherwise replenished the ISM, slowly decreasing the star formation in cluster galaxies (Balogh & Morris, 2000). Strangulated galaxies have higher stellar metallicites in comparison to RPS galaxies of comparable mass, and Peng et al. (2015) used this to determine that strangulation is the dominant form

of quenching for low mass galaxies ($M_* \leq 10^{11} M_\odot$).

Starvation is a similar process but prevents the hot halo from cooling, again halting the replenishment of the cold gas reservoir. This process is usually attributed to the hot temperatures of the ICM, and results in quenching timescales comparable to cold gas depletion times (e.g. Balogh et al., 2000; Fillingham et al., 2015). While starvation has been found to be an important prerequisite for suppressing star formation in most galaxies, it is likely not the sole quenching mechanism driving galaxy evolution (Trussler et al., 2020).

Galaxy-Galaxy Interactions

While the above environmental quenching mechanisms are driven by the interaction of satellite galaxies and the surrounding ICM, more direct interactions between individual galaxies in groups and clusters can also induce quenching. Frequent high speed encounters between satellite galaxies, referred to as "galaxy harassment", are known to be a suitable mechanism for generating significant morphological changes (Moore et al., 1996, 1998, 1999). These tidal interactions are more efficient closer to cluster centres, and can result in the formation of dwarf spheroidal galaxies (Moore et al., 1999; Mastropietro et al., 2005; Smith et al., 2010a; Bialas et al., 2015). In addition, galaxy harassment may trigger star formation activity due to the accumulation of gas in the galaxy centre (Fujita, 1998).

Galaxy interactions may result in the coalescence of galaxies through mergers. These events are typically divided into two broad categories based on the mass ratio between the interacting galaxies; minor mergers are those with mass ratios greater than 1 : 4, while major mergers refer to mergers between galaxies of comparable

Figure 1.8: HST image of the Antennae galaxies NGC 4038 (top) and NGC 4039 (bottom) currently undergoing a major merger in the NGC 4038 Group (Image credit: ESA/Hubble & NASA).

mass (Lotz et al., 2011). Mergers can also be gas rich (wet), where the abundance of star forming gas triggers episodes of starburst activity (e.g. Barton et al., 2000; Lambas et al., 2003; Woods et al., 2006; Petersson et al., 2023) or they can be gas poor (dry), where there is little gas available to make new stars and star formation is limited (Robotham et al., 2013). The nearest major merger between two spiral galaxies is the Antennae (NGC 4038/29, Arp 244), shown in Figure 1.8. This is a wet merger where the most intense star formation is found in the overlap region between both central nuelci (Mirabel et al., 1998; Zhang et al., 2010). As with many galaxies that undergo major mergers, the Antennae will likely form an ultra luminous infrared galaxy in the future (Sanders & Mirabel, 1996; Gao et al., 2001).

Mergers preferentially occur in dense environments compared to the field, and dry mergers in particular are thought to be critical in the mass assembly of present day

red galaxies (Lin et al., 2010; Oogi & Habe, 2013). Overall, mergers are more common in groups compared to clusters due to the lower relative velocities between satellite galaxies, and mergers are more commonly found at higher redshifts (Gottlöber et al., 2001; Lin et al., 2008; Jian et al., 2012).

1.3.3 Outline of this Thesis

The study of galaxy evolution has become a primary branch of astronomy over the last century, yet there are still many unanswered questions. In broad terms, blue, actively star forming spiral galaxies transform into red, quenched ellipticals over time. This transformation is known to take place in dense environments, however the dominant mechanisms driving this evolution are not well constrained.

In this thesis, I am interested in the environmental effect groups and clusters have on galaxy star formation rate and morphology. Specifically, I want to understand the timescales associated with the changes in these two properties and determine which one changes more quickly. By studying the effect of two different environments compared to the field, I can also constrain the amount of pre-processing affecting galaxies on average. In Chapter 2 I use galaxy position in projected phase space as a proxy for time since infall to investigate how star formation rate and morphology change in groups and clusters. I calculate quenching and morphological transformation timescales for SDSS galaxies, and discuss the quenching mechanisms most likely driving this evolution. I summarize my main findings in Chapter 3, and include a discussion on my planned future work. Chapter 2 is the unchanged version of a paper that I have submitted to the refereed astronomical journal titled *Monthy Notices of the Royal Astronomical Society.*

Chapter 2

Satellite Quenching and Morphological Transformation in Galaxy Groups and Clusters

This chapter represents an unchanged version of the paper titled *Satellite Quenching and Morphological Transformation in Galaxy Groups and Clusters*, submitted to the refereed journal *Monthy Notices of the Royal Astronomical Society* by the following authors:

M. Oxland[1], L. C. Parker[1], R. R. de Carvalho,[2], V. M. Sampaio,[2,3]

[1]*Department of Physics & Astronomy, McMaster University, Hamilton, ON, Canada*

[2]*NAT-Universidade Cidade de São Paulo, 01506-000, São Paulo, SP, Brazil*

[3]*School of Physics and Astronomy, University of Nottingham, University Park, Nottingham NG7 2RD, UK*

Abstract

We investigate the role that dense environments have on the quenching of star formation and the transformation of morphology for a sample of galaxies selected from the Sloan Digital Sky Survey. We make a distinction between galaxies falling into groups ($13 \leq \log(M_{\rm halo}/M_{\odot}) < 14$) and clusters ($\log(M_{\rm halo}/M_{\odot}) \geq 14$), and compare to a large sample of field galaxies. Using galaxy position in projected phase space as a proxy for time since infall, we study how galaxy specific star formation rate (sSFR) and morphology, parameterized by the bulge-to-total light ratio (B/T), change over time. After controlling for stellar mass, we find clear trends of increasing quenched and elliptical fractions as functions of infall time for galaxies falling into both groups and clusters. The trends are strongest for low mass galaxies falling into clusters. By computing quenching and morphological transformation timescales, we find evidence that star formation quenching occurs faster than morphological transformation in both environments. Comparing field galaxies to recently infalling galaxies, we determine there is pre-processing of both star formation and morphology, with pre-processing affecting star formation rates more strongly. Our analysis favours quenching mechanisms that act quickly to suppress star formation, while other mechanisms that act on longer timescales transform morphology through bulge growth and disc fading.

2.1 Introduction

Galaxies have long been observed to be largely bimodal in their properties, where the majority of galaxies are either (1) blue in colour, gas-rich, and have high star formation rates (SFRs) or are (2) red in colour, gas-poor, and have low SFRs (e.g. Strateva et al., 2001; Kauffmann et al., 2003a,b; Baldry et al., 2004a; Balogh et al., 2004a,b). It is generally accepted that these two distinct populations represent different stages in galaxy evolution, where blue spiral galaxies have younger stellar populations compared to red elliptical galaxies (González Delgado et al., 2015). Galaxies which have properties intermediate to these two distinct classes populate a region known as the green valley, which typically contains galaxies undergoing star formation quenching and experiencing a transformation in morphology from spiral to elliptical (Martin et al., 2007). The green valley contains relatively few galaxies, suggesting that the quenching of star formation likely occurs quickly especially for elliptical galaxies (Salim, 2014; Schawinski et al., 2014).

Understanding the mechanisms driving star formation quenching and morphological transformation requires a large sample of galaxies which span a variety of stellar masses and environments. The quiescent fraction of galaxies is known to increase with stellar mass, where low mass galaxies are typically star-forming while higher mass galaxies are more quiescent (e.g. Peng et al., 2010b; Wetzel et al., 2012). The quiescent fraction also shows a clear trend with local environment and scales with halo mass, where more quenched galaxies are found in more massive haloes (e.g. Wetzel et al., 2012). Even within individual galaxy clusters, satellites closer to the cluster centre have lower star formation rates than those further out (Balogh et al., 1998; Roberts et al., 2019). These trends suggest there are both internal and environmental

quenching mechanisms that act in transforming galaxies over cosmic time.

When a galaxy is in isolation, galaxy evolution is driven by internal processes. Outflows from Active Galactic Nuclei (AGN) and supernovae feedback can eject cold gas out of the disc and/or heat central gas. This reduces the abundance of cold gas and subsequently suppresses star formation (e.g. Bower et al., 2006; Croton et al., 2006; Agertz et al., 2013). The presence of galactic bars can drive gas into central regions, increasing central star formation (e.g. Hawarden et al., 1986; Wang et al., 2012; Cheung et al., 2013) and inducing bulge growth (Kormendy & Kennicutt, 2004). The growth of a stellar bulge can further stabilize the disc against fragmentation, reducing star formation through morphological quenching (Martig et al., 2009). However, most galaxies in the universe do not live in isolation.

Small groups are the most common environment for galaxies in the local universe (e.g. Eke et al., 2005). Galaxies living in these small groups and larger galaxy clusters are subject to external transformation mechanisms in addition to the internal ones listed above. For example, a satellite galaxy passing through the dense intracluster medium (ICM) may experience a wind that is strong enough to strip cold gas from the galactic disc via ram pressure stripping (RPS) (e.g. Gunn & Gott, 1972). In some cases, RPS can first compress cold gas and trigger an episode of enhanced star formation prior to complete gas removal (Vulcani et al., 2018; Roberts & Parker, 2020). If ram pressure is strong enough, it may eventually strip away all the cold star-forming gas causing the galaxy to quench on relatively short timescales (< 1 Gyr; Quilis et al. (2000)). Other environmental effects may strip only the hot halo, or starvation may prevent the hot gas from cooling, leading to the quenching of star formation as the cold gas reservoir is no longer being replenished (Larson et al.,

1980; Peng et al., 2015). Dynamical interactions such as repeated nearby encounters between nearby galaxies (Moore et al., 1996) or mergers can also affect satellite SFRs and morphologies.

To further complicate the picture of galaxy evolution, the growth of structure in the universe is a hierarchical process where massive galaxy clusters are built up by the accretion of smaller galaxy groups. As a result, many satellite galaxies experience pre-processing in which they have previously been affected by a group environment prior to entering their current cluster (e.g. Fujita, 2004; De Lucia et al., 2012; Wetzel et al., 2015a; Bianconi et al., 2018). Observationally, Hou et al. (2014) found that the observed quiescent fraction in massive clusters is dominated by pre-processed subhaloes, a result in agreement with simulations (e.g. Bahé et al., 2013; McGee et al., 2009). Therefore, constraining both pre-processing and environmental quenching mechanisms is imperative to elucidate the processes driving galaxy evolution in dense environments.

One useful parameter to study how galaxy properties change when evolving through dense environments is the infall time: the time since a galaxy first crossed the virial radius of its present-day host halo (Pasquali et al., 2019). The direct way to measure infall time is to use phase space, a 6D position and velocity space commonly used to study dynamical systems. Galaxies falling into groups/clusters have well defined trajectories through phase space (see fig. 1 of Rhee et al., 2017), but observationally we are limited to projected phase space (PPS). PPS is constructed with projected quantities (i.e line of sight velocities and projected distances from the cluster centre), where infall times can be extracted from cosmological simulations. Recent infalling satellites have larger velocity offsets with respect to the cluster centre, while ancient

infallers are closer to the cluster centre and have small line-of-sight velocities. Using location in PPS for a large sample of galaxies, we can study how galaxy properties change over time.

In recent observational studies, galaxy properties have been shown to correlate strongly with position in PPS. Mahajan et al. (2011) found that at a given projected distance from the cluster centre, the stellar mass and star formation properties of galaxies depend on their absolute line of sight velocity with respect to the cluster centre. Muzzin et al. (2014) studied a population of poststarburst galaxies and showed that they have a distinct distribution in PPS when compared to quiescent and star-forming cluster galaxies. Barsanti et al. (2018) found that passive galaxies dominate the virilaized regions of PPS in both group and cluster environments. Analyses of PPS have been carried out using simulations as well, for example Jaffé et al. (2015) used cosmological simulations to study the effect of ram pressure and determined that there is a specific location in PPS where stripped galaxies are likely to be found. These examples showcase that PPS is a valuable tool when studying galaxy evolution.

In this work, we use the relationship between location in PPS and infall time to provide direct measurements of how SFR and morphology change with time. We build on the previous work of Sampaio et al. (2022) by including an analysis for both group and cluster environments, and we measure the timescales associated with changes in SFR and morphology. We also compare our results to field galaxies enabling us to measure the amount of pre-processing affecting galaxies of different stellar masses and in different environments. Our paper is structured as follows: in Section 2.2 we define the catalogues from which we extract our galaxy sample, in Section 2.3 we explain the methods we use in setting up PPS and assigning infall times to our galaxies. In

Section 2.4 we present our results on how galaxy SFR and morphology change as a function of infall time for galaxies in groups and clusters. We discuss and interpret our results in Section 2.5, and present a summary of our results in Section 2.6. This paper assumes flat, ΛCDM cosmology with $\Omega_M = 0.3$, $\Omega_\Lambda = 0.7$, and $H_0 = 70\,\mathrm{kms^{-1}Mpc^{-1}}$.

2.2 Data

We select galaxies from the Sloan Digital Sky Survey Data Release 7 (SDSS DR7; Abazajian et al., 2009), and limit our sample to local galaxies with z $\leq$ 0.1.

2.2.1 Galaxy groups/clusters from the Yang Group Catalogue

In order to classify galaxies according to their environment, we adopt the Yang Group Catalogue (Yang et al., 2007). This catalog uses a modified version of the halo-based group finder algorithm to identify galaxy groups from the New York University Value-Added Galaxy Catalogue (NYU-VAGC; Blanton et al., 2005). Yang et al. (2007) first identify the centres of potential groups and estimate their characteristic luminosity. The authors then estimate the mass, size, and velocity dispersion of the dark matter halo associated with each group, which they use to determine membership in redshift space. This process is then preformed iteratively until there are no further changes in group membership. Each group is assigned two halo mass estimates: one based on characteristic luminosity and the other based on characteristic stellar mass. We use the halo mass estimated from luminosity in this work, and define galaxy groups to have dark matter haloes with $13 \leq \log(M_{\mathrm{halo}}/M_\odot) < 14$, while galaxy clusters are

those with $\log(M_{\rm halo}/M_{\odot}) \geq 14$. We select galaxy groups/clusters with at least 3 members (N $\geq$ 3) for our main sample.

Unlike the traditional friends-of-friends method, this halo-based group finder can identify groups with only one member (N=1). This enables us to create a supplemental dataset of field galaxies which provides us with a control sample that are not currently experiencing environmental effects.

2.2.2 SFRs and stellar masses from GALEX-WISE

We use SFR and stellar mass measurements from the medium-deep version 2 of the GALEX-SDSS-WISE Legacy Catalogue (GSWLC-2; Salim et al., 2016, 2018), which is a value-added catalogue for SDSS galaxies within the GALEX footprint (Martin et al., 2005). GSWLC-2 derives stellar masses and SFRs from UV+optical+mid-IR SED fitting done using the CIGALE code (Boquien et al., 2019). For this work, we only keep galaxies with stellar masses of $\log(M_{\star}/M_{\odot}) \geq 9$. We define quenched galaxies as those with $\log(\text{sSFR}) < -11\text{yr}^{-1}$, a common value used in the literature, to distinguish star-forming and passive galaxies (Salim et al., 2016).

2.2.3 Morphological classification

To separate early-type from late-type galaxies, we use the bulge to total light ratio (B/T) as a measure of morphology. Unlike visual morphology, this measure is quantitative in nature as it is determined through surface brightness profile fitting. B/T is defined as the fraction of total flux coming from the bulge of the galaxy, so B/T = 0 is a pure disc galaxy while B/T = 1 is a completely bulge-dominated galaxy.

We adopt the B/Ts presented in the UPenn SDSS PhotDec Catalog (Meert

et al., 2015). Briefly, this catalogue performed 2D decompositions in the g, r, and i bands for each of the de Vaucouleurs, Sersic, de Vaucouleurs+Exponential and Seric+Exponetial models for 7×10^5 galaxies in the SDSS DR7. We adopt the r band fits for the de Vaucouleurs bulge and Exponential disc fit for our analysis. The fits were done by Meert et al. (2015) done using the fitting routine GALFIT (Peng et al., 2002) and analysis pipeline PYMORPH (Vikram et al., 2010), which generates a number of physically motivated flags. Meert et al. (2015) flag "bad galaxies" as those with catastrophically bad estimates of total magnitude and radius; we follow the author's recommendation and remove these galaxies from our sample.

Previous studies found that a quantitative definition of early-type galaxies should be based on B/T and image smoothness (S) (e.g. Im et al., 2002; Tran et al., 2003). We therefore apply a cut in S since elliptical galaxies are expected to be relatively smooth and symmetric. We use the r-band image smoothness parameters presented in Simard et al. (2011) as an additional parameter when defining elliptical galaxies. $S = R_T + R_A$, where R_T and R_A are calculated following Eq. 11 of Simard et al. (2002) and represent the amount of light in symmetric and asymmetric components, calculated from the fitting model. Simard et al. (2009) determined that a good definition of early-type galaxies that matches well to visual classifications are those with B/T ≥ 0.35 and S ≤ 0.075. However, in this work we are interested primarily in elliptical (E) galaxies but there is no clear way to distinguish E's from S0's using B/T alone. We use a slightly more conservative cut of B/T ≥ 0.5 with S ≤ 0.075 to define E's for this work. This choice removes some S0's, but we note our sample of ellipticals is still contaminated by S0's.

We cross match the environment, SFR, and morphology catalogues together and

remove any galaxies with invalid measurements of mass, SFRs, or halo mass (i.e. null/ NaN/ 0). In Section 2.3 we explain further steps taken to define the set of galaxies in groups and clusters used in this analysis.

2.3 Methods

2.3.1 Projected Phase Space

We locate galaxies in projected phase space (PPS) by plotting the line of slight velocity as a function of projected radial distance for each galaxy, both with respect to clustercentric coordinates. We normalize the x and y axes by the cluster's virial radius (R_{180}) and 1D velocity dispersion (σ_{1D}), respectively, in order to create a stacked version of PPS containing galaxies in groups and clusters. For consistency, we follow the Yang et al. (2007) definitions:

$$\sigma_{1D} = 397.9 \text{km s}^{-1} \left(\frac{M_h}{10^{14} h^{-1} M_\odot} \right)^{0.3214} \tag{2.3.1}$$

$$R_{180} = 1.26 h^{-1} \text{Mpc} \left(\frac{M_h}{10^{14} h^{-1} M_\odot} \right)^{1/3} (1 + z_{\text{group}})^{-1} \tag{2.3.2}$$

Where M_h is the halo mass and z_{group} is the redshift of the group/cluster centre.

We adopt the "new zones" determined by Pasquali et al. (2019) to correlate position in PPS with a time since infall (T_{inf}). The authors define T_{inf} as "the time since a galaxy crossed for the first time the virial radius of the main progenitor of its present-day host environment". They used the Yonsei Zoom in Cluster Simulations (YZiCS) to derive zones of constant mean infall time for galaxies in each region of

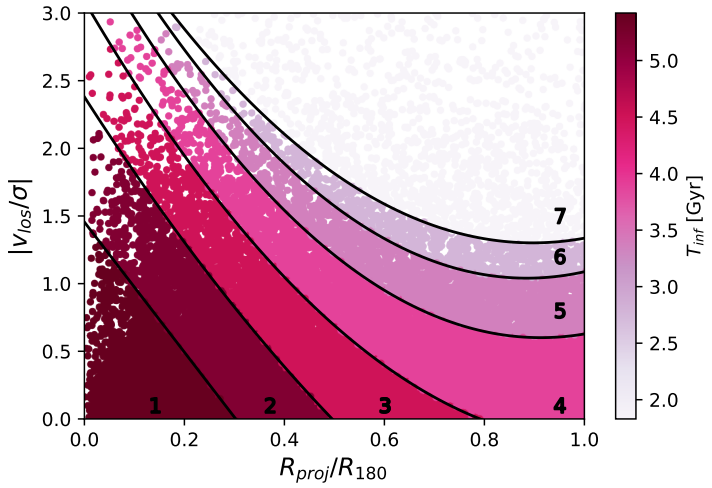

Figure 2.1: Projected phase space diagram for all our galaxies in groups and clusters. The colour bar distinguishes the 7 different regions determined by Pasquali et al. (2019), where the corresponding infall times are provided in Table 2.1.

PPS. The zones defined by Pasquali et al. (2019) are valid for $|v_{\rm los}|/\sigma_{\rm 1D} \leq 3$ and $R_{\rm proj}/R_{180} \leq 1$, which reduces our parent sample of galaxies in groups and clusters. The authors also divide PPS into 8 different zones, but we note their zone 7 is quite narrow so we combine their zones 7 and 8 into a single region with a corresponding mean infall time of 1.83 Gyr. For each zone, the mean infall time and standard deviations are listed in Table 2.1, and the PPS for our galaxy sample is shown in Fig. 2.1.

2.3.2 Populating the outskirts of projected phase space

To improve the statistics within zones 6 and 7, we add additional galaxies to the outskirts of our groups and clusters that may not have been identified as members by the halo-based group finder of Yang et al. (2007). We do so by finding all isolated galaxies (N=1) that are within 1 R_{180} of a galaxy group centre, and then determine

Table 2.1: Projected phase space zone number (see Fig. 2.1), the corresponding time since infall, and the associated standard deviations of T_{inf}. The numerical values are determined from simulations (Pasquali et al., 2019).

Zone	T_{inf} [Gyr]	$\sigma(T_{inf})$ [Gyr]
1	5.42	2.51
2	5.18	2.60
3	4.50	2.57
4	3.89	2.34
5	3.36	2.36
6	2.77	2.29
7	1.83	2.47

the line-of-sight velocity relative to this new cluster centre. We normalize these measurements by equations (2.3.1) & (2.3.2), and keep those within $|v_{los}|/\sigma_{1D} \leq 3$ and $R_{proj}/R_{180} \leq 1$. This added 608 galaxies to our sample, 95% of which are located within zones 6 and 7.

Our final sample of galaxies in PPS contains 23665 galaxies, of which 14713 are in groups and 8952 are in clusters. For our field sample, we remove any galaxies in the Yang N=1 data set within $3R_{180}$ of a group or cluster. This results in a sample of 79108 field galaxies.

2.4 Results

It is well known that galaxies accreting into groups and clusters both decrease their star formation rate and experience a morphological transformation from disc to bulge-dominated. However, there is currently no clear consensus as to the physical mechanisms driving these changes, or the timescales associated with such processes. In this section, we explore both the quenched and elliptical fraction of galaxies as functions of time since infall to better constrain the physical mechanisms driving galaxy evolution

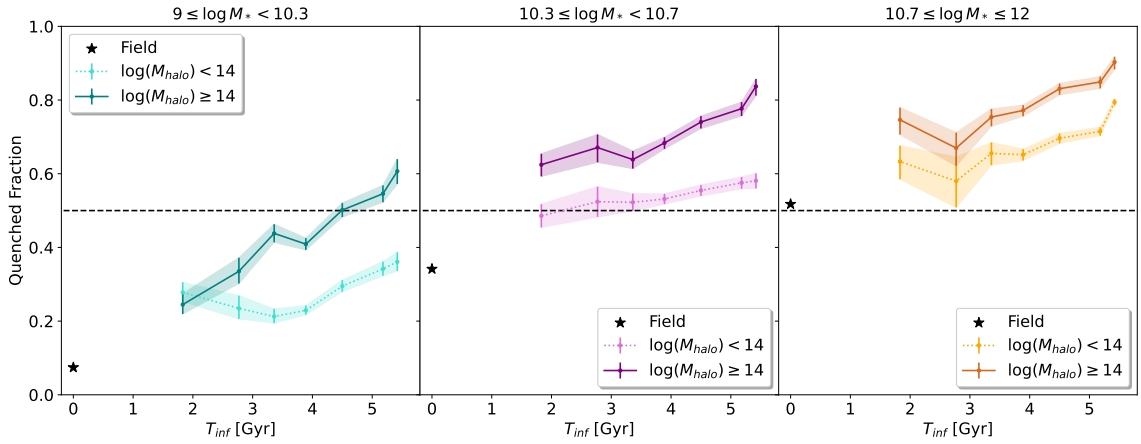

Figure 2.2: The quenched fraction of galaxies as a function of time since infall. The left most panel corresponds to low mass galaxies, while the middle and right most panels contain intermediate and high mass galaxies, respectively. The dotted lines in each panel represent the galaxies in groups, while solid lines are galaxies in clusters. The error bars corresponding to the 68% confidence intervals estimated from the beta distribution (Cameron, 2011). Black stars represent field galaxies and are artificially placed at $T_{inf} = 0$, and have uncertainties that are smaller than the marker size. Finally, the black dashed line represents the point at which 50% of galaxies in a given class are quenched.

through dense environments. Since galaxy properties are known to correlate with stellar mass and host halo mass (eg. Kauffmann et al. (2003b); Peng et al. (2010b); Wetzel et al. (2012)), we separate our analysis into three stellar mass bins and two environments.

2.4.1 Quenched Fraction

In Fig. 2.2 we show the quenched fraction (QF; $\log(\text{sSFR}) < -11\text{yr}^{-1}$) as a function of time since infall, where T_{inf} is determined based on galaxy position in PPS (see Fig. 2.1). The three panels correspond to low ($9 \leq \log(M_\star/M_\odot) < 10.3$), intermediate ($10.3 \leq \log(M_\star/M_\odot) < 10.7$), and high ($10.7 \leq \log(M_\star/M_\odot) < 12$) mass galaxies,

chosen to have approximately the same number of galaxies in each mass bin. Within each panel we separate galaxies into those within groups ($13 \leq \log(M_{\rm halo}/M_{\odot}) < 14$) and clusters ($\log(M_{\rm halo}/M_{\odot}) \geq 14$). In addition, we artificially plot the quenched fraction of field galaxies at $T_{\rm inf}$=0 to compare galaxies evolving through dense environments to those in the field. Note there are a minimum of 50 galaxies in each $T_{\rm inf}$ bin.

The QF increases over time for galaxies falling into group and cluster environments, although the trends are stronger in clusters compared to groups. The population with the steepest slope are low mass galaxies in clusters, suggesting these galaxies are the most strongly affected by their environment. The dashed horizontal line at QF=0.5 indicates the separation between where most galaxies are star-forming (QF$<$ 0.5) or quiescent (QF$>$ 0.5), and is used to calculate the quenching timescales (see Section 2.4.3). Interestingly, most low mass galaxies in groups and clusters are actively star-forming 1.83 Gyr after infall, while intermediate and high mass galaxies are typically already quenched (see discussion of pre-processing in Section 2.5.4). We also note that the QF for intermediate and high mass galaxies appears to remain relatively flat until 3.36 Gyr, and then starts to increase. This could suggest these galaxies experience a delay phase followed by a decrease in their star formation rate, consistent with the delayed then rapid quenching scenario (e.g. Wetzel et al., 2013; Rhee et al., 2020).

Unsurprisingly and in agreement with many previous works (e.g. Wetzel et al., 2012, 2013), the QF depends both on stellar mass and environment where the lowest fractions are found in the field and increase with stellar mass and halo mass. For completeness, we show the trend of sSFR as a function of $T_{\rm inf}$ in Fig. 2.9.

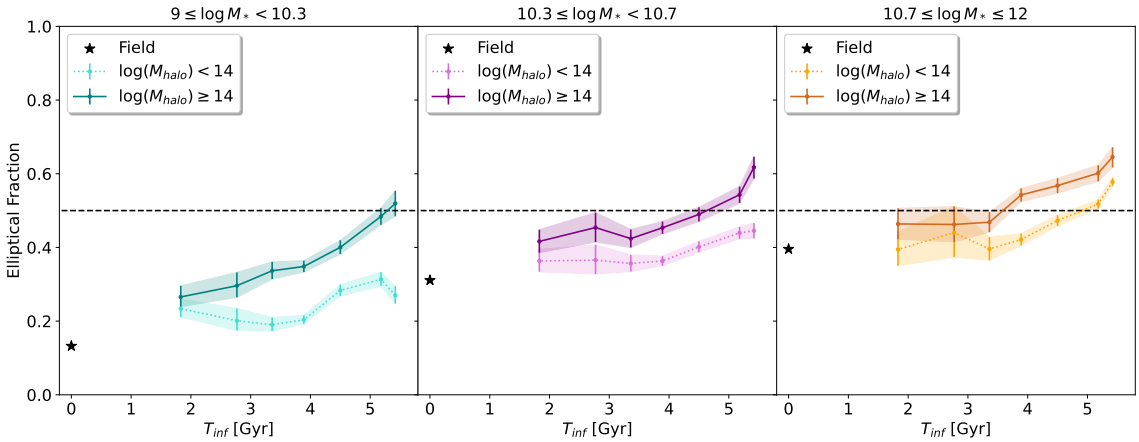

Figure 2.3: The elliptical fraction of galaxies as a function of time since infall. The separate panels and colours are the same as those defined in Fig. 2.2, with error bars corresponding to the 68% confidence intervals estimated from the beta distribution (Cameron, 2011). The error bars on the field populations are smaller than the black star marker, and the black dashed line represents the point at which 50% of galaxies in a given class are considered elliptical.

2.4.2 Elliptical Fraction

In Fig. 2.3 we plot the elliptical fraction (EF; B/T ≥ 0.5 and S ≤ 0.075) as a function of T_{inf}. The EF bears a striking resemblance to the QF in Fig. 2.2. For all galaxy populations, the EF increases as a function of T_{inf} and it depends on both stellar mass and halo mass. The steepest slope corresponds once again to low mass galaxies falling into clusters. The dashed horizontal line at EF=0.5 is the division between where most galaxies are disc dominated (EF$<$ 0.5) or elliptical (EF$>$ 0.5), and is used when calculating the morphological transformation timescales in Section 2.4.3. In general, most galaxies fall into environments as disc-dominated systems and slowly become elliptical over time. However, low and intermediate mass galaxies in groups are typically disc dominated for the entire time they are a part of their group. The field is dominated by galaxies with disc morphologies.

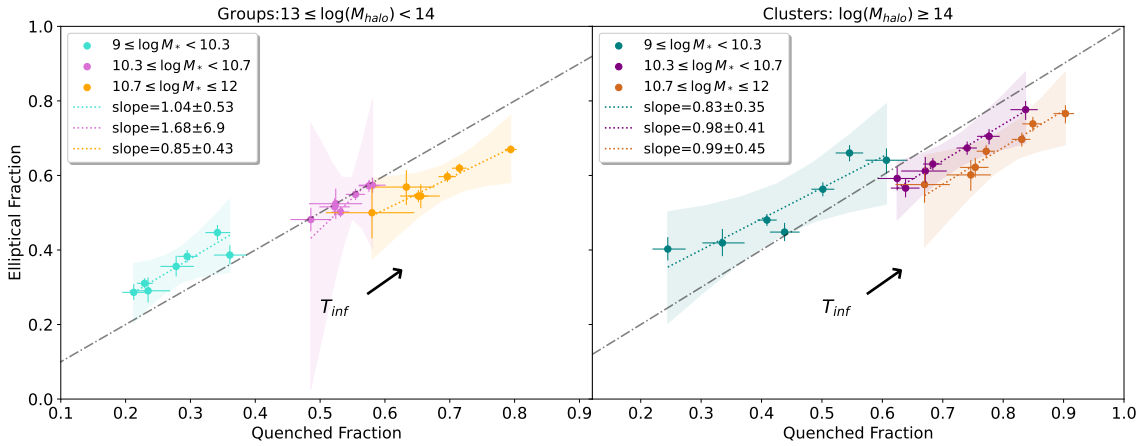

Figure 2.4: The elliptical fraction as a function of the quenched fraction. The left and right panels correspond to galaxies in groups and clusters, respectively, while galaxies in different stellar mass bins are represented by the different coloured points. Each data point corresponds to a specific time since infall, where T_{inf} increases from the bottom left to the top right as shown by the illustrative black arrow. The linear least squares fit to each population is shown by dotted lines, where the slope of each line is provided in the legend. The error bars on each data point correspond to the 68% confidence intervals estimated from the beta distribution (Cameron, 2011), and the shaded regions show the 95% confidence interval of the best-fitting line from LINMIX (Kelly, 2007). The dot-dash line shows the one-to-one line.

We again note intermediate and high mass galaxies have EFs that remain quite flat up until 3.36 Gyr before increasing, supporting the delayed then rapid quenching scenario. For completeness, we provide a plot of the median B/T as a function of T_{inf} in Fig. 2.10. The overall trends are the same as the ones presented in this section.

2.4.3 What happens first: quenching or morphological transformation?

In the previous sections, we explored how the QF and EF change over time as galaxies fall into groups and clusters. In this subsection, we combine the results from Sections

2.4.1 and 2.4.2 in an attempt to address the question whether it is star formation quenching or morphological transformation that occurs first. We first do so by plotting the EF as a function of the QF, as shown in Fig. 2.4. Each data point corresponds to one specific T_{inf}, where T_{inf} increases from the bottom left to the top right as shown by the illustrative black arrow.

In Fig. 2.4 we see that as galaxies fall into groups and clusters, the elliptical and quenched fractions both increase as expected. Within groups, the elliptical fraction and quenched fraction systematically increase with increasing stellar mass. For clusters on the other hand, there is significant overlap between intermediate and high mass galaxies. For each population we use the hierarchical Bayesian model LINMIX (Kelly, 2007) to determine the best-fitting straight line, taking into account the errors in both fractions. The slopes of the resultant best-fitting lines are provided in the legend. With large error bars in the best-fitting lines, it is difficult to determine from this analysis alone if star formation or morphology changes more quickly.

An alternative approach we take in addressing this question is to compute the physical timescales associated with quenching and morphological transformation. We define the quenching timescale as the time it takes for a specific galaxy population to have a QF=0.5. We do so by fitting a simple linear least squares fit to each subpopulation in Fig. 2.2, taking into account the uncertainty on the QF, and determine at what T_{inf} value the quenched fraction crosses the dashed line. Similarly, we define the morphological transformation timescale as the T_{inf} at which a specific galaxy population has an EF=0.5, calculated from Fig. 2.3. Both timescales are plotted in Fig. 2.5.

Within each stellar mass range we find that morphological transformation timescales

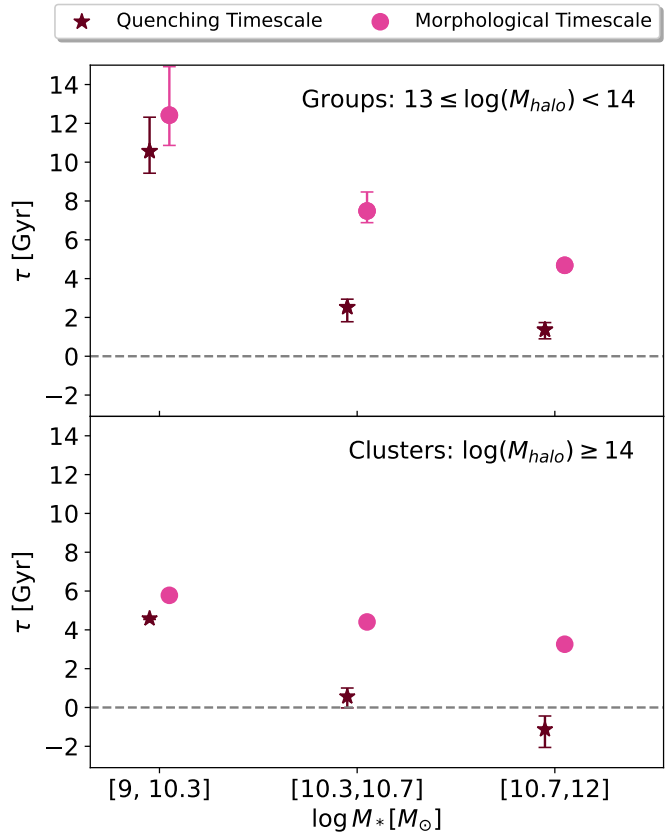

Figure 2.5: The quenching and morphological transformation timescales for low ($9 \leq \log(M_\star/M_\odot) < 10.3$), intermediate ($10.3 \leq \log(M_\star/M_\odot) < 10.7$), and high ($10.3 \leq \log(M_\star/M_\odot) < 12$) mass galaxies in groups (top) and clusters (bottom). The quenching timescales are plotted as burgundy stars, while the morphological transformation timescales are plotted as pink circles. The errors are calculated from the formal uncertainty of the slope and y-intercept of the best-fitting line.

are longer than quenching timescales, suggesting quenching happens prior to morphological transformation. Both timescales also decrease with increasing stellar mass, and the timescales are shorter in clusters when compared to galaxies of comparable mass in groups. Low mass galaxies in groups have extremely long timescales ($\geq$ 9 Gyr), suggesting these galaxies do not show significant signs of either quenching or morphological transformation. High mass galaxies in clusters have negative quenching timescales, and although this may seem nonphysical, it points to significant pre-processing of star formation prior to becoming satellites of their current cluster environment. We discuss the effects of pre-processing further in Section 2.5.4.

The T_{inf} associated with each PPS zone has a large standard deviation (see Table 1), which were not considered when calculating the linear fits. This should be kept in mind when interpreting our results.

2.5 Discussion

In this paper we investigate the environmental effect of groups and clusters on galaxy star formation rates and morphologies to help constrain the timescales associated with satellite quenching and morphological transformation. Similar to previous work, our findings suggest that clusters have the most influence on galaxy sSFR and morphology, with low mass galaxies being the most susceptible to environmental effects. In terms of both the QF and EF, galaxies in both groups and clusters of all stellar masses show a clear offset from the field. This indicates galaxies have likely experienced pre-processing prior to entering their current host environment. In the following sections we interpret our results and discuss the physical mechanisms that may be driving galaxy evolution through dense environments.

2.5.1 Evidence for star formation quenching prior to morphological transformation

Our goal in this work was to answer the question of whether it is star formation quenching or morphological transformation that happens first for galaxies falling into groups and clusters. By looking at the elliptical fraction as a function of the quenched fraction in Fig. 2.4, we determine that both fractions are increasing as a function of infall time, but it is difficult to disentangle which is changing first due to large uncertainty. We expand upon this analysis by calculating the quenching and morphological transformation timescales (see Fig. 2.5). We find evidence that star formation quenching is changing prior to morphological transformation, with the exception of low mass galaxies in groups. These galaxies have extremely long timescales (≥ 9 Gyr), suggesting they do not show any evidence of quenching or significant morphological changes while they are a satellite of a group environment.

Our results agree with several recent studies that use PPS. Kelkar et al. (2019) used observational data from the ESO Distant Cluster Survey (White et al., 2005) and found a correlation between stellar age and position in PPS, irrespective of morphology. They argue this is evidence star formation is suppressed earlier than morphology. Martínez et al. (2023) reached the same conclusion for cluster galaxies; they separated galaxies into five dynamical classes based on their position in PPS and compared the fraction of ellipticals and passives to an interloper population (see Section 2.5.2 for a quantitative comparison). Our results disagree with those by Martig et al. (2009) and Sampaio et al. (2022), who used cosmological simulations and SDSS observations, respectively. Martig et al. (2009) argue morphological transformation and star

formation quenching occur simultaneously, and attribute the changes to morphological quenching. Sampaio et al. (2022) use galaxy position in PPS and T-Type as a measure of morphology to study how sSFRs and morphologies change over time in galaxy clusters. By plotting T-Type versus sSFR, they find a greater change in morphology compared to sSFR over a fixed time interval, arguing that this is evidence morphology is changing more rapidly than sSFR.

Our analysis is similar to that of Sampaio et al. (2022) with a number of differences. Firstly, we use B/T as a measure of morphology instead of T-Type. T-Type is a measurement that comes from Convolutional Neural Networks calibrated with Galaxy Zoo 2 data (Domínguez Sánchez et al., 2018; Willett et al., 2013), while B/T is calculated from photometric decompositions. While both are common morphology indicators, they are not perfectly correlated and may be the origin of our differing results. Secondly, the comparison of T-Type and sSFR is difficult to interpret as the two measures have differing units (see their fig. 10). Our choice to explore the QF versus the EF removes units, making comparisons between the changes in star formation and morphology more straight-forward. To make a direct comparison to fig. 10 of Sampaio et al. (2022), we provide a plot of B/T as a function of sSFR in Fig. 2.11. It appears sSFR is changing more quickly than morphology, but again note the difficultly in comparing changes in B/T and sSFR.

The quenching timescales we calculate provide us with a quantitative way to determine how SFRs change both as a function of stellar mass and environment. However, making direct comparisons to work in the literature is difficult due to the many ways quenching timescales are defined (see Cortese et al. (2021) for a review). Our quenching timescales are defined as the time from $T_{inf}=0$ to the time the population has a

QF=0.5 (see Section 2.4.3). We find that quenching timescales decrease with increasing stellar mass, and they are longer in groups compared to clusters. The timescale for low mass galaxies in groups of $\geq$ 9 Gyr suggests these galaxies are likely not quenching in their current group environment.

Several works have tried to constrain satellite quenching timescales and have come to similar conclusions. De Lucia et al. (2012) used a semi-analytic model applied to the merger trees of the Millennium Simulation (Springel et al., 2005), computing quenching timescales of 5-7 Gyrs and determining there is significant pre-processing of cluster galaxies. Wetzel et al. (2013) used both SDSS observations and cosmological simulations to study the star formation histories of galaxies falling into clusters. They proposed the "delayed-then-rapid" quenching model, where satellites experience little to no change in their SFRs for 2-4 Gyrs, after which they experience rapid star formation quenching ($\leq$ 1 Gyr). These timescales were found to be shorter at higher stellar masses, and they found the observed increase in the quiescent fraction with host halo mass is due to group pre-processing. Oman & Hudson (2016) used N-body simulations and SDSS galaxies in PPS to estimate quenching timescales. They accounted for pre-processing effects and found that all galaxies quench on their first infall, within 1 Gyr of their first pericentric passage. They find higher mass satellites quench earlier, with little dependence on host cluster mass.

Although there is no one definition of quenching timescale used in the literature, the overall trend of decreasing quenching timescales with increasing stellar mass is clear. We find shorter quenching timescales in clusters compared to group environments, but explore the possibility this is due to pre-processing in Section 2.5.4.

We acknowledge that the specific timescales calculated here are dependent on the

definition of EF, QF, and the thresholds chosen. For example, if we chose a more conservative cut of B/T$\geq$0.7 for our elliptical galaxy definition, the morphological transformation timescales all increase. Alternatively, the quenching timescales decrease if we use a lower log(sSFR) threshold to define quenched galaxies. For this reason it is the overall trends with stellar mass, halo mass, and the comparison between the morphological transformation and quenching timescales that are meaningful, rather than the exact numerical timescales calculated. Since morphological transformation timescales depend on the measure of morphology used, future work is needed to better understand these differences.

2.5.2 Evolution of cluster galaxies: more evidence for quenching prior to morphological change

Recently, Martínez et al. (2023) studied galaxies within bright X-ray clusters to explore how sSFR and morphology change over time. They apply the code ROGER (De los Rios et al., 2021), which uses three different Machine Learning techniques to classify galaxies into one of five orbital classes based on position in PPS. The five dynamical classes are cluster galaxies, recent infallers, backsplash galaxies, infallers, and interlopers. Based on the results of De los Rios et al. (2021), Martínez et al. (2023) adopt the K-Nearest Neighbour technique to compute class probabilities. Their sSFRs come from the MPA-JHU DR7 catalogue (Brinchmann et al., 2004), and their morphological classifications are from the Galaxy Zoo Project (Lintott et al., 2008). The authors use the probabilities of being elliptical (P_E) or spiral (P_S) from Lintott et al. (2011a), and consider a galaxy to be elliptical if $P_E > P_S$.

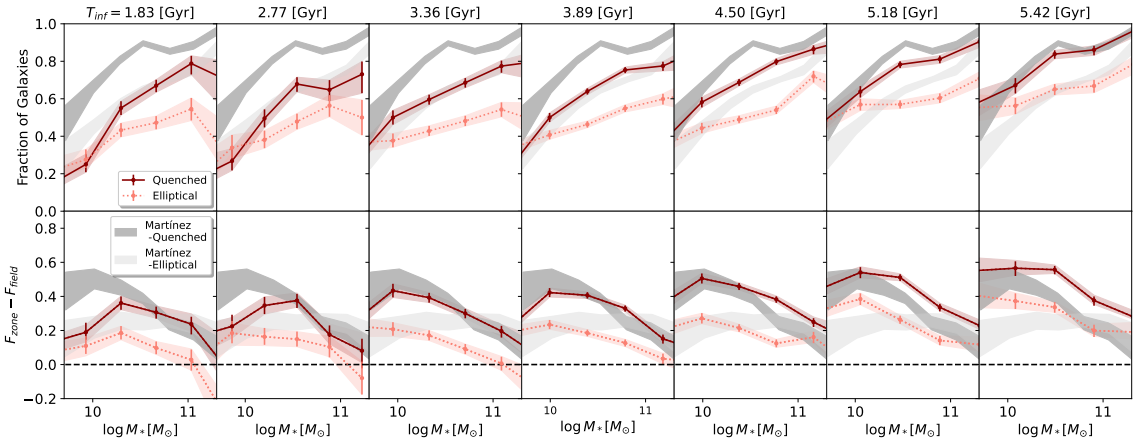

Figure 2.6: The top row shows the fraction of ellipticals (salmon coloured dotted line), and fraction of quenched galaxies (burgundy solid line) as a function of stellar mass, with each panel representing a specific T_{inf} labeled at the top of each plot. Error bars correspond to the 68% confidence intervals estimated from the beta distribution (Cameron, 2011). In the bottom panel we show the difference of the elliptical fraction and quenched fraction relative to the fractions in our field sample. The horizontal black dashed line is plotted at $F_{\rm zone} - F_{\rm field}$=0. The elliptical fraction (dark grey) and passive fraction (light grey) for the cluster galaxies from fig. 7 of Martínez et al. (2023) are plotted in the background.

Martínez et al. (2023) compare the fraction of ellipticals to the fraction of passives within each of their five predicted classes as a function of galaxy stellar mass (see their fig. 7). Interlopers are analogous to a field population, while the sequence of infallers, recent infallers, backsplash, and cluster galaxies corresponds roughly to time since infall. They find quenching is enhanced as soon as galaxies fall into clusters, while significant morphological transformations require longer periods of time. The authors come to this conclusion as it takes longer for the fraction of elliptical galaxies to significantly deviate from the field compared to the fraction of passives.

Since the progression from infallers to cluster galaxies traces galaxies through PPS, I can compare our work to the work of Martínez et al. (2023) using the 7 zones of our PPS (see Fig. 2.1). We plot the elliptical fraction and quenched fraction of cluster galaxies as a function of stellar mass, where each panel corresponds to one T_{inf} bin in Fig. 2.6. We plot the results for the cluster galaxy classification of Martínez et al. (2023) in the background, as this is the classification our PPS diagram overlaps the most with. We again consider a galaxy to have an elliptical morphology if $B/T \geq 0.5$ and $S \leq 0.075$, and to be quenched if $\log(\text{sSFR}) \leq -11\text{yr}^{-1}$.

The top row of Fig. 2.6 shows both the EF and QF increase as a function of stellar mass. The fractions increase the longer a galaxy has been a part of a cluster, supporting the idea that environment has an effect on both SFR and morphology. Quenched fractions are also systematically larger than elliptical fractions over all T_{inf} bins.

In the bottom row of Fig. 2.6 we show the difference of the fractions in the upper row compared to the fractions of our field sample. At all T_{inf}, the QF is consistently above the EF at all stellar masses. As T_{inf} increases, the QF continues

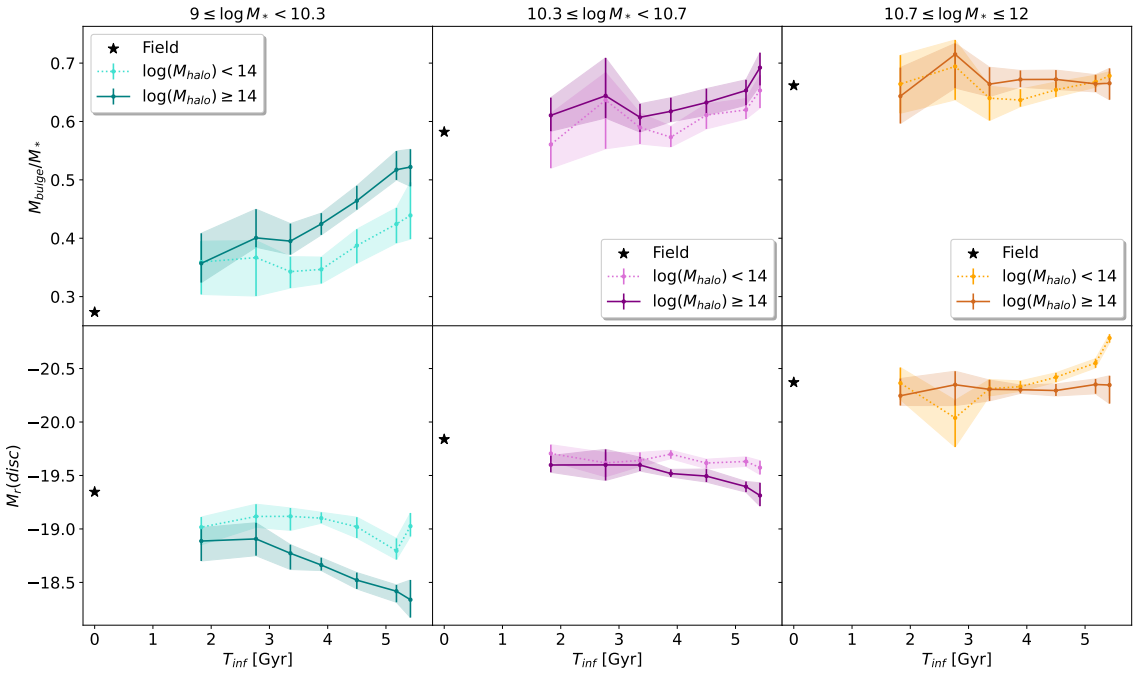

Figure 2.7: Top: The median bulge mass fraction of galaxies as a function of time since infall. Bottom: The median absolute magnitude of the disc as a function of time since infall. The separate panels and colours are the same as those defined in Fig. 2.2, with error bars showing the 90% confidence interval from 1000 bootstrap iterations.

to deviate from the field, while it takes longer for the EF to deviate significantly. Specifically, at T_{inf} =2.77 Gyr the QF is already above the dashed line, while the EF takes 4.5 Gyr to differ from the field at all stellar masses. These results strengthen our previous conclusion that it takes a shorter time to quench a cluster galaxy than it does to transform its morphology from disc to bulge-dominated. These findings are consistent with Martínez et al. (2023).

2.5.3 Bulge growth and disc fading quenching mechanisms

It has been a topic of recent works whether it is bulge growth or disc fading that is responsible for the transformation of galaxy morphology in dense environments (e.g Head et al., 2014; Quilley & de Lapparent, 2022). However, looking at B/T alone it is impossible to disentangle the effects of bulge growth from disc fading as both lead to an increase in B/T. In this section, we explore bulge mass fraction and disc magnitudes as a function of time since infall to study how the bulge and disc behave separately, and to constrain the mechanisms driving morphological change.

Bulge mass fraction ($M_{\rm bulge}/M_\star$) provides a continuous number between 0 and 1 that specifies how bulge dominated a galaxy is. For our work, we adopt the bulge and disc mass estimates from Mendel et al. (2014) who extended the catalogue of Simard et al. (2011) to include u-, i-, and j-band photometry. Mendel et al. (2014) determine bulge, disc, and total mass estimates from fitting bulge+disc and Sersic profile photometric decompositions. They note the total masses derived from the bulge+disc fit (M_{B+D}) can deviate from the sum of the independently derived bulge and disc masses ($M_B + M_D$) when photometric uncertainties are high. The authors suggest removing galaxies with overestimated bulge masses, identified where the offset between M_{B+D} and $M_B + M_D$ is greater than 1σ. We remove these galaxies from our sample and use $M_B + M_D$ when calculating the bulge mass fraction. Cross matching our sample to this catalogue results in a final sample of 22132 galaxies in groups and clusters, and 69560 field galaxies.

Bulge mass fraction as a function of $\rm T_{inf}$ is plotted in the top row of Fig. 2.7. The overall trends are similar to Fig. 2.10, where low mass galaxies in clusters show the strongest trend with $\rm T_{inf}$. As galaxy stellar mass increases, the offset between galaxy

groups and clusters becomes less pronounced and the trends with T_{inf} flatten. The low mass field galaxies have smaller bulge mass fractions than group and cluster galaxies, but field galaxies become increasingly similar to the group and cluster galaxies with increasing stellar mass. We explore disc fading in the bottom row of Fig. 2.7. Here, we plot the disc r-band absolute magnitudes ($M_{r(\mathrm{disc})}$ from Meert et al. (2015)) as a function of T_{inf}. For the lowest mass galaxies there is significant disc fading in clusters. The rest of the galaxy populations appear to show little to no change in $M_{r(\mathrm{disc})}$ over time.

By looking at bulge mass fraction and disc magnitudes in Fig. 2.7, it appears both bulge growth and disc fading drive morphological transformation. Low mass galaxies in clusters experience the strongest change over time in both bulge mass fraction and disc magnitude, however it is not possible in this analysis to disentangle which of the two is primarily responsible for changes in morphology.

Several different environmental quenching mechanisms may be responsible for the cessation of star formation, the growth of galaxy bulges, and the fading of galaxy discs. Bulge-enhancing mechanisms tend to drive gas into the galaxy centre, possibly feeding a supermassive black hole and quenching star formation through AGN feedback in high mass galaxies (Schawinski et al., 2006, 2007; Head et al., 2014). Often, mergers within groups/in the field and repeating galaxy interactions within clusters can explain this scenario (Boquien et al., 2019; Quilley & de Lapparent, 2022; Moore et al., 1996), as well as the morphological disruption of galaxy discs.

Mechanisms effecting the amount of gas in a galaxy's disc can lead to disc fading, and recently both RPS and starvation have been favoured as primary satellite quenching mechanisms (Wetzel et al., 2015b). RPS can directly strip cold gas from

the disc, removing gas that could have otherwise formed stars. This process can quench galaxies on short timescales (< 1 Gyr; Quilis et al., 2000) while having little to no effect on overall galaxy morphology. However, RPS is thought to play an important role in the fading of galaxy discs as it preferentially strips gas near the edges of a galaxy. This can lead to long HI tails and the apparent truncation of HI discs (Chung et al., 2007). Starvation results in a reduced accretion rate of halo gas onto the disc, limiting the amount of gas available for future star formation. Both RPS and starvation are consistent with our analysis, although the morphological evolution of galaxies may also be driven by other environmental mechanisms such as mergers and interactions.

2.5.4 Pre-processing of star formation and morphology

In Section 2.4.3 we found that morphological transformation timescales are longer than quenching timescales, which are both shorter in clusters compared to groups. A common explanation for why quenching timescales are shorter in high density environments is pre-processing (Wetzel et al., 2013). In this section, we investigate the effect of pre-processing on star formation and morphology for galaxies falling into groups and clusters.

To quantify the amount of pre-processing affecting SFR in this work, we calculate the difference in the field QF and the first T_{inf} bin from Fig. 2.2 for each stellar mass and environment. We calculate the amount of pre-processing affecting morphology similarly, using the field EF and first T_{inf} data point in Fig. 2.3. The pre-processed fractions for group and cluster environments are shown in Fig. 2.8. Overall, pre-processing has an effect on both morphology and star formation, yet star formation is

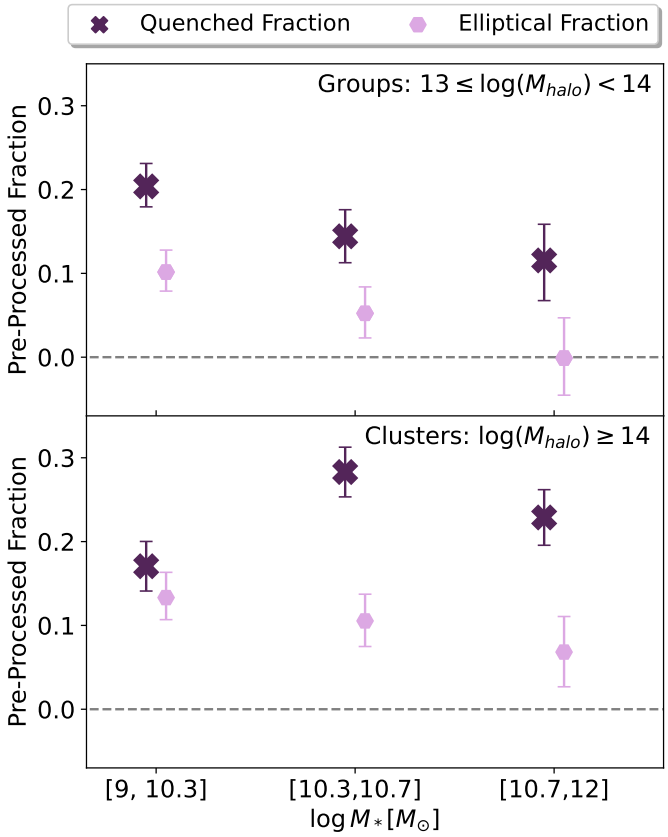

Figure 2.8: The pre-processed fraction for low, intermediate, and high mass galaxies in groups (top) and clusters (bottom). The pre-processed fraction associated with star formation and morphology are plotted as dark purple crosses and light purple hexagons, respectively. The errors represent the 1σ uncertainty calculated from the 68 % confidence interval of the first data point at T_{inf} =1.83Gyr in Figs. 2.2 and 2.3.

more strongly pre-processed. We find the fraction of pre-processed galaxies in groups ranges from 10-20% when considering the quenched fraction, and 0-10% when considering the elliptical fraction. The pre-processed fractions also decrease with increasing stellar mass, and both fractions are comparable or slightly larger for clusters.

Prior studies have attempted to constrain the effects of pre-processing either by tracing galaxy evolution through simulations or observationally by measuring substructure in galaxy clusters. Bahé et al. (2013) use the GIMIC suite of high-resolution hydrodynamic simulations and find the fraction of galaxies that have been satellites of a previous halo of mass $> 10^{13} M_{\odot}$ ranges from $< 10\%$ to 60% for galaxies currently in haloes of mass $\leq 10^{13.5} M_{\odot}$ and $10^{15.2} M_{\odot}$, respectively. Using the YZiCS, Jung et al. (2018) study the gas content of satellite galaxies in clusters with masses ranging from $5 \times 10^{13} < M_{200}/M_{\odot} < 15$. They find evidence that 34% of their galaxies are gas poor prior to entering their current cluster environment. Haines et al. (2015) model satellite infall applied to observations in an attempt to recreate the known trend of star-forming fraction and cluster-centric radius. The authors find that recently infalling galaxies have a star-forming fraction that is reduced by 19% compared to the field.

In terms of galaxy morphology, Wilman et al. (2009) study the fraction of S0-type galaxies in group and field environments at z$\sim$0.4. They find an excess of S0s at fixed luminosity in groups compared to the field, and beyond $0.3 h_{75}^{-1}$ Mpc from group centres. They find this hints at pre-processing playing an important role in the formation of S0 galaxies. More recently, Brambila et al. (2023) find a statistically significant difference in the asymmetry and smoothness parameters between field and cluster galaxies, finding evidence for pre-processing affecting galaxy morphology as

well as star formation.

Roberts & Parker (2017) used observational data from the SDSS to make direct comparisons between the pre-processing of star formation and morphology. The authors quantify the degree to which star-forming fractions and disc fractions are suppressed in dense environments compared to the field for low and high mass galaxies. Qualitatively, they found evidence of both the pre-processing of star formation and morphology, although could not say for certain if one is more strongly pre-processed than the other. Quantitatively, they find the fraction of pre-processed low-mass galaxies ranges between 4-11% for star-forming fraction and 4-7% for disc fractions, which both decrease for higher mass galaxies. The largest pre-processed fractions are found in low mass galaxies falling into high mass haloes. Our results are generally in agreement qualitatively, although our low mass galaxies in clusters have smaller pre-processed fractions compared to intermediate and high mass galaxies in clusters. This is not surprising looking at Fig. 2.2, and may be driven by large uncertainties in infall time.

2.6 Summary & Conclusions

In this work we investigate the environmental effect of galaxy groups and clusters on the star formation rate and morphology of 23665 galaxies in the Sloan Digital Sky Survey Data Release 7. We use location in projected phase space as a proxy for time since infall to study the timescales associated with star formation quenching and morphological transformation. We separate our galaxies into three stellar mass bins (low: $9 \leq \log(M_\star/M_\odot) < 10.3$, intermediate: $10.3 \leq \log(M_\star/M_\odot) < 10.7$, and high: $10.7 \leq \log(M_\star/M_\odot) < 12$), and distinguish between galaxies in groups

($13 \leq \log(M_{\rm halo}/M_{\odot}) < 14$) and clusters ($\log(M_{\rm halo}/M_{\odot}) \geq 14$). We compare our results to a sample of 79108 field galaxies, and study how the quenched and elliptical fractions of galaxies change over time as galaxies fall into groups and clusters. Our main findings are as follows:

- Changes in both the quenched fraction and elliptical fraction depend on stellar mass and environment, where we find clear evidence of increasing QF and EF as functions of $\rm T_{inf}$. The strongest trends are found for low mass galaxies falling into clusters.

- By comparing the quenching and morphological transformation timescales in Section 2.4.3, we find that morphological timescales are longer than quenching timescales in both groups and clusters. This supports the idea that quenching occurs faster than morphological transformation in both environments. However, low mass galaxies show no signs of significant quenching or morphological transformation in group environments (timescales are ≥ 9 Gyr).

- By comparing the QF and EF of recently infalling galaxies to our field population in Section 2.5.4, we find evidence for the pre-processing of both star formation rate and morphology, with pre-processing having a stronger effect on star formation. The pre-processing fractions typically decrease with increasing stellar mass, and slightly increase in clusters compared to groups

- Our analysis favours quenching mechanisms that act quickly to suppress sSFR, and act on longer timescales to grow galaxy bulges and fade galaxy discs. Possible mechanisms that quench star formation are RPS and starvation, while mergers and galaxy interactions may drive morphological evolution.

Acknowledgements

LCP would like to thank the Natural Science and Engineering Council of Canada for funding. MO thanks M. Bravo, L. Foster, and D. Lazarus for helpful discussions. This work was made possible thanks in large part to number of publicly available software packages, including Astropy (Astropy Collaboration et al., 2022), Matplotlib (Hunter, 2007), Numpy (Harris et al., 2020), Pandas (McKinney et al., 2010), SciPy (Virtanen et al., 2020), and Topcat (Taylor, 2005).

Funding for the Sloan Digital Sky Survey V has been provided by the Alfred P. Sloan Foundation, the Heising-Simons Foundation, the National Science Foundation, and the Participating Institutions. SDSS acknowledges support and resources from the Center for High-Performance Computing at the University of Utah. The SDSS web site is www.sdss5.org.

SDSS is managed by the Astrophysical Research Consortium for the Participating Institutions of the SDSS Collaboration, including the Carnegie Institution for Science, Chilean National Time Allocation Committee (CNTAC) ratified researchers, the Gotham Participation Group, Harvard University, The Johns Hopkins University, L'Ecole polytechnique fédérale de Lausanne (EPFL), Leibniz-Institut für Astrophysik Potsdam (AIP), Max-Planck-Institut für Astronomie (MPIA Heidelberg), Max-Planck-Institut für Extraterrestrische Physik (MPE), Nanjing University, National Astronomical Observatories of China (NAOC), New Mexico State University, The Ohio State University, Pennsylvania State University, Smithsonian Astrophysical Observatory, Space Telescope Science Institute (STScI), the Stellar Astrophysics Participation Group, Universidad Nacional Autónoma de México, University of Arizona, University of Colorado Boulder, University of Illinois at Urbana-Champaign,

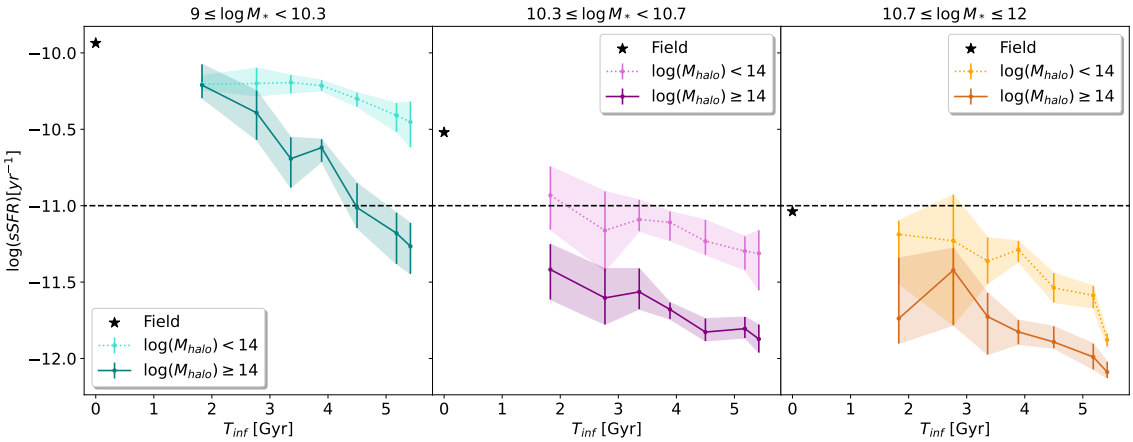

Figure 2.9: The median sSFR as a function of time since infall. The separate panels and colours are the same as those defined in Fig. 2.2. The error bars show the 90% confidence interval from 1000 bootstrap iterations, and black dashed line at $\log_{10}(\text{sSFR}) = -11\text{yr}^{-1}$ represents our distinction between star-forming and quenched galaxies.

University of Toronto, University of Utah, University of Virginia, and Yale University.

Data Availability

Galaxies used in this analysis were selected from the SDSS-DR7. Group and cluster membership was taken from the Yang Group Catalogue. Galaxy specific star formation rates were calculated from the star formation rates and stellar mass estimates of GSWLC-2, while B/T morphology measurements came from the SDSS PhotDec Catalogue. Smoothness parameters are from Simard et. al. 2011, and the bulge mass fractions were calculated from Mendel et. al. 2014.

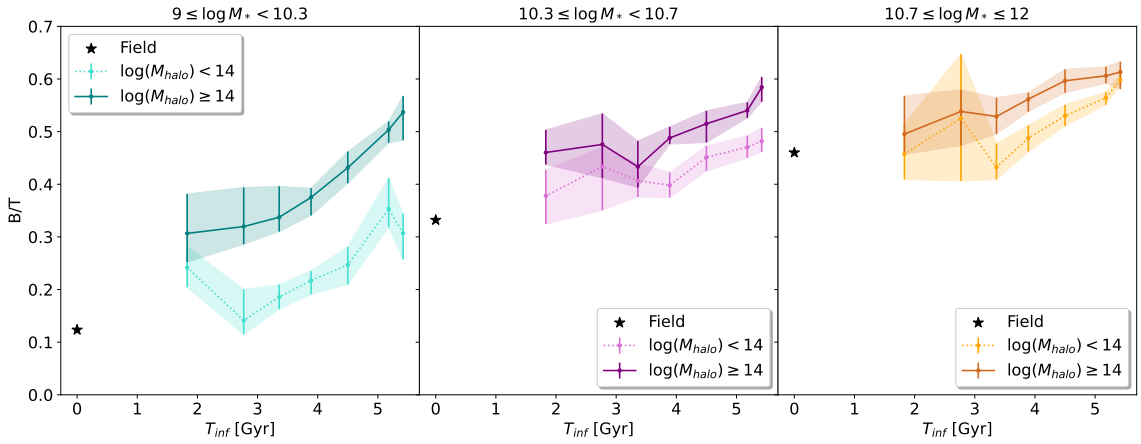

Figure 2.10: The median B/T as a function of time since infall. The separate panels and colours are the same as those defined in Fig. 2.2, with errors showing the 90% confidence interval from 1000 bootstrap iterations.

2.7 Appendix A: Star Formation Quenching

To complement the quenched fraction shown in Fig. 2.2, in Fig. 2.9 we plot median galaxy sSFR as a function of T_{inf}. Over time, sSFRs decrease as satellite galaxies fall into both groups and cluster environments. Trends are strongest for low mass galaxies falling into clusters.

2.8 Appendix B: Morphological Transformation

To complement the elliptical fraction shown in Fig. 2.3, in Fig. 2.10 we plot the median B/T as a function of T_{inf}. As galaxies fall into groups and clusters, B/Ts increase and galaxies become more bulge dominated. Once again, the trends are strongest for low mass galaxies in clusters.

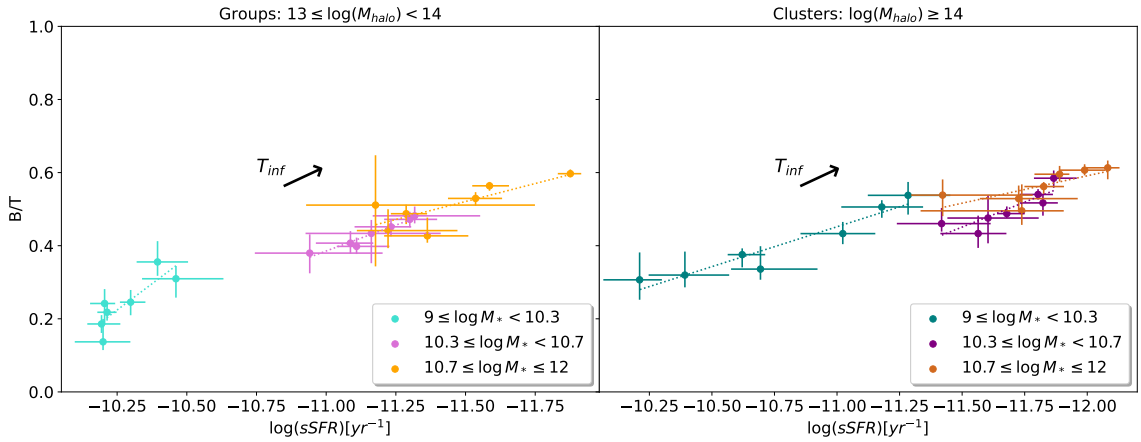

Figure 2.11: B/T versus sSFR. The left and right panels correspond to galaxies in groups and clusters, respectively, while galaxies in different stellar mass bins are represented by different coloured points shown in the legend. Time since infall increases from the bottom left to top right, represented by the illustrative black arrow. The linear least squares fit to each population is shown by dotted lines, and the error bars represent the 90% confidence intervals from 1000 bootstrap iterations.

2.9 Appendix C: B/T vs. Specific Star Formation Rate

In Fig. 2.11, we show B/T versus sSFR for galaxies in groups (left) and clusters (right). As stated in Section 2.4.3, the comparison between B/T and sSFR is difficult to interpret as the two variables have different units, but plotted in this way enables us to make comparisons to fig. 10 of Sampaio et al. (2022). Over time, B/T increases while sSFR decreases, as expected. It appears there is a greater change in sSFR compared to B/T, suggesting quenching occurs prior to significant changes in morphology.

Chapter 3

Summary & Conclusions

Galaxies have intrigued scientists ever since their discovery almost a century ago, and while several questions about the nature of galaxies have been answered, there is a growing list of open research questions that remain. In particular, a fundamental question regarding galaxy evolution has been the central focus of several works over the past few decades: what mechanisms are driving the evolution of galaxies through dense environments? This is the question that this thesis aims to address.

In Chapter 2 we studied the environmental impact of galaxy groups and clusters on the star formation rate and morphology for 23665 SDSS galaxies. We defined quenched galaxies as those with $\log(\text{sSFR}) < -11\text{yr}^{-1}$, elliptical galaxies as those with $\text{B/T} \geq 0.5$ and $\text{S} \leq 0.075$, and used location in projected phase space as a proxy for time since infall. Our general trends of how SFR and morphology change with environment are consistent with the discussion of Section 1.2. In particular, we find more quenched galaxies in massive halos (i.e. clusters have the most quenched galaxies, the field has the fewest) where clusters also have the most elliptical galaxies. By studying the trends of the quenched fraction and elliptical fraction with T_{inf}, we

find both fractions increase over time the longer a galaxy is in a group or cluster. The strongest trends are found for low mass galaxies falling into clusters (see Figures 2.2 and 2.3), suggesting low mass galaxies are the most impacted by their environment.

These initial findings support galaxy environment having a significant impact on both SFR and morphology, however there is still debate about the timescales associated with these changes (Cortese et al., 2021). By determining the T_{inf} at which the quenched and elliptical fractions cross a threshold of 50%, we were able to study the timescales associated with star formation quenching and morphological transformation. Quenching timescales are shorter than morphological transformation timescales for galaxies of comparable mass in both groups and clusters (see Figure 2.5), suggesting quenching happens prior to significant morphological change. However, low mass galaxies in groups show no signs of quenching or morphological change because their timescales are so high ($\geq$ 9 Gyr). Our method using the QF and EF is novel, and therefore cannot easily be compared to other authors who have also measured timescales. However, the overall trend of decreasing quenching timescales with increasing galaxy stellar mass has been found before (e.g. Wetzel et al., 2013; Oman & Hudson, 2016).

It is also important to point out our conclusions are dependent on the exact thresholds chosen when defining quenched and elliptical galaxies, as discussed in Section 2.5.1. If we select a more conservative cut of B/T when defining elliptical galaxies for example, the morphological timescales all increase. The quenching timescales also decrease if a lower sSFR is chosen for quenched galaxies. It is for this reason we do not put too much emphasis on the exact numerical values calculated, rather the trends with halo mass, stellar mass, and the comparison between quenching and morphology

timescales are what are important.

Pre-processing has been shown to suppress galaxy SFRs and play a major role in the observed fraction of ETGs in galaxy clusters (e.g. Kautsch et al., 2008; Sengupta et al., 2022) By comparing to a sample of field galaxies, we are able to constrain the amount of pre-processing affecting current group and cluster galaxies. We find that pre-processing affects both galaxy SFR and morphology in both environments, but has a slightly stronger effect on SFR (see Figure 2.8). These results are in agreement with Roberts & Parker (2017), who were able to quantify the amount of pre-processing affecting satellite galaxies by comparing the star forming fraction and disc fraction of cluster galaxies to that of the field.

Our work builds upon the work of previous groups who attempted to use PPS to study galaxy evolution through clusters. Sampaio et al. (2022) used the same PPS zones from Pasquali et al. (2019) with different SFR and morphology indicators. They found that morphology appears to change more quickly than SFRs, a result in direct contrast to our work. However, our results are in agreement with numerous other studies who utilized PPS. One example is Martínez et al. (2023) who used different PPS regions and found the same conclusion that SFRs change more quickly (see Section 2.5.2 for a direct comparison). Other recent works with similar qualitative results include Kelkar et al. (2019); Rhee et al. (2020); Jeon et al. (2022); Lopes et al. (2024).

Our analysis provides support for RPS and starvation driving galaxy quenching, while mergers and galaxy interactions may drive morphological transformation through bulge growth and disc fading (see Section 2.5.3). This analysis proves galaxy evolution is a complex process driven by a combination of environmental mechanisms,

and while our analysis is valuable and supports claims made by others, more work can be done to fully understand how galaxies evolve in dense environments.

3.1 Future Work

One limitation of our work was the specific zones of PPS we decided to adopt. While it is well known location in PPS correlates well to the average time a galaxy has been a part of it's current environment (Rhee et al., 2017), there are a number of different ways PPS can be split up. For example, Rhee et al. (2017) separate PPS into 5 distinct regions (labeled A-E, see their fig. 6) however the exact time since infall of each region is not well constrained. Caustic profiles and radial bins have also been used to separate galaxies at different stages of infall (e.g. Gill et al., 2005; Mahajan et al., 2011), but Pasquali et al. (2019) found that these two methods do not accurately trace the accretion history of clusters. Instead, Pasquali et al. (2019) define eight "new zones" of PPS that better follow the true infall distribution of their simulated galaxies.

These "new zones" are the ones we adopt for this work, where the main advantage is that there is an average T_{inf} provided for each zone. However, we note a number of possible issues that may arise from choosing these phase space regions. Firstly, the standard deviation of T_{inf} is large within each zone (see Table 2.1), and is not taken into account in our analysis. Secondly, these zones were calibrated using the Yonsei Zoom-in Cluster Simulations where the halo masses only range from $5.3 \times 10^{13} - 9.2 \times 10^{14} M_{\odot}$. This works well when applied to our cluster galaxies, but may not translate well to less massive structures. Therefore, our groups which have significantly lower halo masses ($13 \leq \log(M_{\rm halo}/M_{\odot}) < 14$) may actually have different infall times than

massive clusters, affecting our results. Thirdly, these PPS zones are only well defined within $1 \times R_{\rm vir}$, cutting off our analysis to only galaxies relatively close to the cluster centre. While having an observational tool such as PPS provides observers with a useful way to study the accretion history of galaxies, the weaknesses discussed above suggest there are a number of improvements needing to be made. One natural path moving forward includes the calibration of PPS down to group scales and to larger cluster-centric radii.

Groups are the most common environment in the local universe (Eke et al., 2005), however they are harder to identify compared to massive clusters and are therefore less well studied. One future project arising from this thesis is the calibration of PPS down to group scales. Since clusters grow by accreting smaller groups, this will fill a much needed gap in galaxy evolution studies. To do this, hydrodynamic galaxy simulations can be used to trace galaxy evolution through group environments and subsequently define PPS zones. The method will be similar to that of Pasquali et al. (2019), where each region of group PPS is associated with an average time since infall. These PPS zones can then be used with observational data to study the evolution of group satellite galaxies over time. This will in turn improve our analysis of pre-processing, as we will have a more accurate way of studying the prior group environments of cluster galaxies.

In addition, simulations are required to extend the calibrated PPS zones out to larger cluster-centric radii. Our current analysis is limited to $1 \times R_{\rm vir}$, but recent works have found evidence that environment can impact satellite galaxies much farther away from the central. In particular, several backsplash galaxies (those which have made a pericentric passage and now reside outside of the virial radius) are found between

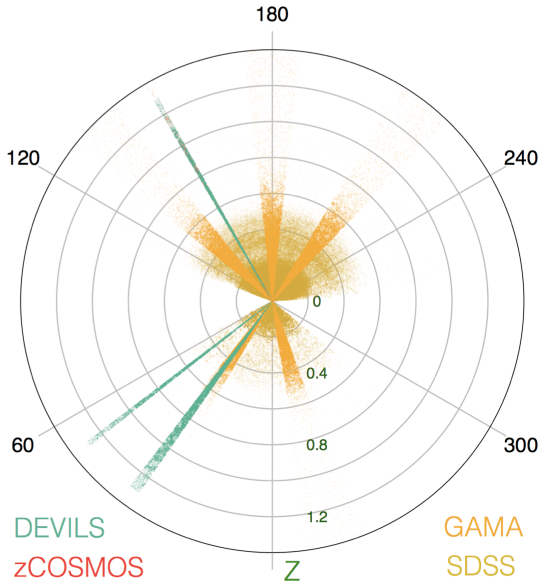

Figure 3.1: Light cone distributions for the SDSS, GAMA, DEVILS, and zCOSMOS. Figure from Davies et al. (2018).

$1 - 2.5 \times R_{\rm vir}$ (e.g. Mamon et al., 2004; Gill et al., 2005). It has also been found that some jellyfish galaxies which are undergoing RPS reside beyond $1 \times R_{\rm vir}$ (Jaffé et al., 2018), and pre-processing has recently been found to have a measurable effect on star formation way out at $5 \times R_{200}$ (Lopes et al., 2024). By extending the PPS zones to larger cluster-centric radii, we will include a large population of galaxies undergoing environmental quenching that were missed in our analysis. In addition, we will be able to better constrain the amount of pre-processing affecting cluster galaxies.

After calibrating PPS to galaxy groups and larger cluster-centric radii, this analysis can be extended to higher redshift samples. Specifically, I will use the Galaxy and Mass Assembly Survey (GAMA; Driver et al., 2011) and the Deep Extragalactic Visible Survey (DEVILS; Davies et al., 2018) which cover redshifts of $z < 0.5$ and $0.2 < z < 1$ respectively (Figure 3.1). These surveys have the advantage of being more complete out to greater distances compared to the SDSS (Davies et al., 2018),

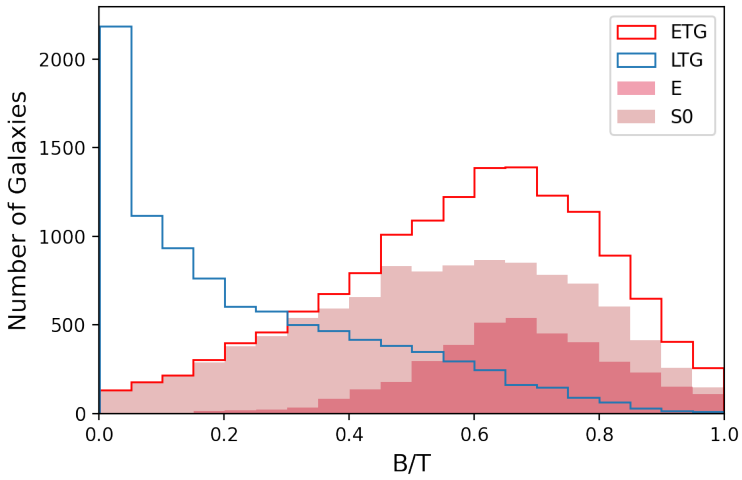

Figure 3.2: Histogram of the B/T for my sample of galaxies, subdivided based on Hubble type morphology from Domínguez Sánchez et al. (2018). Late-type galaxies (T-Type > 0) are in blue, early-types (T-Type ≤ 0) are in red. ETGs are subdivided into ellipticals (light pink) and S0s (dark pink).

and therefore are able to detect more small, faint galaxies in dense environments. These low mass galaxies are the ones most affected by their environment, so having a more complete sample would improve our analysis. Studying higher redshift galaxies is of interest as there is some evidence suggesting quenching timescales decrease with increasing redshift (Foltz et al., 2018). In addition, the dominant environmental quenching mechanism may even change between z=0 and 1 (Balogh et al., 2016). The data sets provided by GAMA and DEVILS will be of great value for a future analysis.

Another part of this thesis that raised questions was that different measures of morphology can lead to varying results. In particular, our results using B/T as a measure of morphology were contradictory to a similar analysis by Sampaio et al. (2022) who used T-Type, an alternative measure of morphology commonly used. It is troubling that different measurements supposedly tracing the same physical

property result in different conclusions, so we explored this topic when preparing the Chapter 2 manuscript. We cross matched our sample of PPS SDSS galaxies (with B/T measurements) to the morphology catalogue of Domínguez Sánchez et al. (2018) (with T-Types and S0 probabilities (PS0)) to see if a B/T cut of 0.5 accurately separates ellipticals from S0s. As shown in Figure 3.2, elliptical galaxies (those with T-Type $\leq$ 0 and PS0 < 0.5) and S0s (those with T-Type ≤ 0 and PS0 > 0.5) overlap significantly in their B/Ts. This makes it difficult to separate the two submorphologies based on B/T alone. Even by imposing a smoothness cut in our definition of elliptical, our sample was still contaminated by S0s. There being no strong correlation between these measurements raises questions as to what the "best" morphology indicator is. An in-depth analysis comparing different morphology indicators is therefore needed in the future.

This thesis has explored the evolution of galaxies through group and cluster environments to shed light on the processes driving star formation quenching and morphological transformation. While our results are in agreement with several other works, our analysis has raised several important questions and opened the floor to various paths moving forward. Using simulations to better calibrate PPS, we will be able to elucidate the evolution of group and cluster galaxies at higher redshifts. With several spectroscopic redshift surveys planned including the 4MOST Hemisphere Survey of the Nearby Universe (4HS; Taylor et al., 2023), the 4MOST eROSITA Galaxy Cluster Redshift Survey (Finoguenov et al., 2019), and the Wide-Area VISTA Extragalactic Survey (WAVES; Driver et al., 2019), group-finding algorithms will only improve and galaxy evolution science will flourish over the next few decades.

Bibliography

Abadi M. G., Moore B., Bower R. G., 1999, MNRAS, 308, 947

Abazajian K., et al., 2003, AJ, 126, 2081

Abazajian K. N., et al., 2009, ApJS, 182, 543

Abbott T. M. C., et al., 2018, ApJS, 239, 18

Agertz O., Kravtsov A. V., Leitner S. N., Gnedin N. Y., 2013, ApJ, 770, 25

Argudo-Fernández M., et al., 2015, A&A, 578, A110

Astropy Collaboration et al., 2022, ApJ, 935, 167

Bahé Y. M., McCarthy I. G., Balogh M. L., Font A. S., 2013, MNRAS, 430, 3017

Baldry I. K., Glazebrook K., Brinkmann J., Ivezić Ž., Lupton R. H., Nichol R. C., Szalay A. S., 2004a, ApJ, 600, 681

Baldry I. K., Balogh M. L., Bower R., Glazebrook K., Nichol R. C., 2004b, in Allen R. E., Nanopoulos D. V., Pope C. N., eds, American Institute of Physics Conference Series Vol. 743, The New Cosmology: Conference on Strings and Cosmology. pp 106–119 (arXiv:astro-ph/0410603), doi:10.1063/1.1848322

Baldry I. K., Balogh M. L., Bower R. G., Glazebrook K., Nichol R. C., Bamford S. P., Budavari T., 2006, MNRAS, 373, 469

Balogh M. L., Morris S. L., 2000, MNRAS, 318, 703

Balogh M. L., Schade D., Morris S. L., Yee H. K. C., Carlberg R. G., Ellingson E., 1998, ApJ, 504, L75

Balogh M. L., Morris S. L., Yee H. K. C., Carlberg R. G., Ellingson E., 1999, ApJ, 527, 54

Balogh M. L., Navarro J. F., Morris S. L., 2000, ApJ, 540, 113

Balogh M., et al., 2004a, MNRAS, 348, 1355

Balogh M. L., Baldry I. K., Nichol R., Miller C., Bower R., Glazebrook K., 2004b, ApJ, 615, L101

Balogh M. L., et al., 2016, MNRAS, 456, 4364

Bamford S. P., et al., 2009, MNRAS, 393, 1324

Barnes A. T., et al., 2023, ApJ, 944, L22

Barsanti S., et al., 2018, ApJ, 857, 71

Barton E. J., Geller M. J., Kenyon S. J., 2000, ApJ, 530, 660

Bell E. F., et al., 2004, ApJ, 608, 752

Bialas D., Lisker T., Olczak C., Spurzem R., Kotulla R., 2015, A&A, 576, A103

Bianconi M., Smith G. P., Haines C. P., McGee S. L., Finoguenov A., Egami E., 2018, MNRAS, 473, L79

Blanton M. R., Moustakas J., 2009, ARA&A, 47, 159

Blanton M. R., et al., 2005, AJ, 129, 2562

Boissier S., 2013, in Oswalt T. D., Keel W. C., eds, , Vol. 6, Planets, Stars and Stellar Systems. Volume 6: Extragalactic Astronomy and Cosmology. p. 141, doi:10.1007/978-94-007-5609-0˙3

Boquien M., Burgarella D., Roehlly Y., Buat V., Ciesla L., Corre D., Inoue A. K., Salas H., 2019, A&A, 622, A103

Boselli A., Fossati M., Sun M., 2022, A&A Rev., 30, 3

Bower R. G., Benson A. J., Malbon R., Helly J. C., Frenk C. S., Baugh C. M., Cole S., Lacey C. G., 2006, MNRAS, 370, 645

Brambila D., Lopes P. A. A., Ribeiro A. L. B., Cortesi A., 2023, MNRAS, 523, 785

Brinchmann J., Charlot S., White S. D. M., Tremonti C., Kauffmann G., Heckman T., Brinkmann J., 2004, MNRAS, 351, 1151

Brooks A., Christensen C., 2016, in Laurikainen E., Peletier R., Gadotti D., eds, Astrophysics and Space Science Library Vol. 418, Galactic Bulges. p. 317 (arXiv:1511.04095), doi:10.1007/978-3-319-19378-6˙12

Bruzual G., Charlot S., 2003, MNRAS, 344, 1000

Cameron E., 2011, PASA, 28, 128

Caon N., Capaccioli M., D'Onofrio M., 1993, MNRAS, 265, 1013

Carnall A. C., McLure R. J., Dunlop J. S., Davé R., 2018, MNRAS, 480, 4379

Carroll B. W., Ostlie D. A., 2017, An Introduction to Modern Astrophysics, 2 edn. Cambridge University Press, doi:10.1017/9781108380980

Cheung E., et al., 2013, ApJ, 779, 162

Chung A., van Gorkom J. H., Kenney J. D. P., Vollmer B., 2007, ApJ, 659, L115

Cortese L., et al., 2007, MNRAS, 376, 157

Cortese L., Catinella B., Smith R., 2021, PASA, 38, e035

Croton D. J., et al., 2006, MNRAS, 365, 11

Davies L. J. M., et al., 2018, MNRAS, 480, 768

De Lucia G., Weinmann S., Poggianti B. M., Aragón-Salamanca A., Zaritsky D., 2012, MNRAS, 423, 1277

De los Rios M., Martínez H. J., Coenda V., Muriel H., Ruiz A. N., Vega-Martínez C. A., Cora S. A., 2021, MNRAS, 500, 1784

Domínguez Sánchez H., Huertas-Company M., Bernardi M., Tuccillo D., Fischer J. L., 2018, MNRAS, 476, 3661

Dressler A., 1980, ApJ, 236, 351

Driver S. P., et al., 2011, MNRAS, 413, 971

Driver S. P., et al., 2019, The Messenger, 175, 46

Eke V. R., Baugh C. M., Cole S., Frenk C. S., King H. M., Peacock J. A., 2005, MNRAS, 362, 1233

Elmegreen B. G., 1998, in Woodward C. E., Shull J. M., Thronson Harley A. J., eds, Astronomical Society of the Pacific Conference Series Vol. 148, Origins. p. 150 (arXiv:astro-ph/9712352), doi:10.48550/arXiv.astro-ph/9712352

Elmegreen B. G., Lada C. J., 1977, ApJ, 214, 725

Fabian A. C., 2012, ARA&A, 50, 455

Fasano G., et al., 2015, MNRAS, 449, 3927

Fillingham S. P., Cooper M. C., Wheeler C., Garrison-Kimmel S., Boylan-Kolchin M., Bullock J. S., 2015, MNRAS, 454, 2039

Finoguenov A., et al., 2019, The Messenger, 175, 39

Foltz R., et al., 2018, ApJ, 866, 136

Fraternali F., 2017, in Fox A., Davé R., eds, Astrophysics and Space Science Library Vol. 430, Gas Accretion onto Galaxies. p. 323 (arXiv:1612.00477), doi:10.1007/978-3-319-52512-9˙14

Fujita Y., 1998, ApJ, 509, 587

Fujita Y., 2001, ApJ, 550, 612

Fujita Y., 2004, PASJ, 56, 29

Fukugita M., et al., 2007, AJ, 134, 579

Gabor J. M., Davé R., Oppenheimer B. D., Finlator K., 2011, MNRAS, 417, 2676

Gao Y., Lo K. Y., Lee S. W., Lee T. H., 2001, ApJ, 548, 172

Gensior J., Kruijssen J. M. D., Keller B. W., 2020, MNRAS, 495, 199

Gill S. P. D., Knebe A., Gibson B. K., 2005, MNRAS, 356, 1327

González Delgado R. M., et al., 2015, A&A, 581, A103

Goto T., Yamauchi C., Fujita Y., Okamura S., Sekiguchi M., Smail I., Bernardi M., Gomez P. L., 2003, MNRAS, 346, 601

Gottlöber S., Klypin A., Kravtsov A. V., 2001, ApJ, 546, 223

Gunn J. E., Gott J. Richard I., 1972, ApJ, 176, 1

Gunn J. E., et al., 1998, AJ, 116, 3040

Haines C. P., et al., 2015, ApJ, 806, 101

Hamilton D., 1985, ApJ, 297, 371

Harris C. R., et al., 2020, Nature, 585, 357

Hashimoto Y., Oemler Augustus J., Lin H., Tucker D. L., 1998, ApJ, 499, 589

Hawarden T. G., Mountain C. M., Leggett S. K., Puxley P. J., 1986, MNRAS, 221, 41P

Head J. T. C. G., Lucey J. R., Hudson M. J., Smith R. J., 2014, MNRAS, 440, 1690

Hernández-Toledo H. M., Avila-Reese V., Salazar-Contreras J. R., Conselice C. J., 2006, AJ, 132, 71

Herschel W., 1786, Phill. Trans. R. Soc, 76, 457

Hester J. A., et al., 2010, ApJ, 716, L14

Hopkins A. M., Beacom J. F., 2006, ApJ, 651, 142

Hou A., Parker L. C., Harris W. E., 2014, MNRAS, 442, 406

Hubble E. P., 1925, Popular Astronomy, 33, 252

Hubble E. P., 1926, ApJ, 64, 321

Hubble E. P., 1936, Realm of the Nebulae

Huchra J. P., Geller M. J., 1982, ApJ, 257, 423

Huertas-Company M., Aguerri J. A. L., Bernardi M., Mei S., Sánchez Almeida J., 2011, A&A, 525, A157

Hunter J. D., 2007, Computing in Science & Engineering, 9, 90

Im M., et al., 2002, ApJ, 571, 136

Jaffé Y. L., Smith R., Candlish G. N., Poggianti B. M., Sheen Y.-K., Verheijen M. A. W., 2015, MNRAS, 448, 1715

Jaffé Y. L., et al., 2018, MNRAS, 476, 4753

Jeon S., et al., 2022, ApJ, 941, 5

Jian H.-Y., Lin L., Chiueh T., 2012, ApJ, 754, 26

Jung S. L., Choi H., Wong O. I., Kimm T., Chung A., Yi S. K., 2018, ApJ, 865, 156

Karachentseva V. E., 1973, Soobshcheniya Spetsial'noj Astrofizicheskoj Observatorii, 8, 3

Kauffmann G., et al., 2003a, MNRAS, 341, 33

Kauffmann G., et al., 2003b, MNRAS, 341, 54

Kautsch S. J., Gonzalez A. H., Soto C. A., Tran K.-V. H., Zaritsky D., Moustakas J., 2008, ApJ, 688, L5

Kelkar K., Gray M. E., Aragón-Salamanca A., Rudnick G., Jaffé Y. L., Jablonka P., Moustakas J., Milvang-Jensen B., 2019, MNRAS, 486, 868

Keller B. W., Wadsley J., Benincasa S. M., Couchman H. M. P., 2014, MNRAS, 442, 3013

Keller B. W., Kruijssen J. M. D., Wadsley J. W., 2020, MNRAS, 493, 2149

Kelly B. C., 2007, ApJ, 665, 1489

Kennicutt Robert C. J., 1992, ApJ, 388, 310

Kennicutt Robert C. J., 1998, ARA&A, 36, 189

Kennicutt R. C., Evans N. J., 2012, ARA&A, 50, 531

Kepple G. R., Sanner G. W., 1998, The night sky obervers guide. Vol. 1, Richmond, Va. : Willmann-Bell

Kormendy J., Kennicutt Robert C. J., 2004, ARA&A, 42, 603

Lambas D. G., Tissera P. B., Alonso M. S., Coldwell G., 2003, MNRAS, 346, 1189

Larson R. B., Tinsley B. M., Caldwell C. N., 1980, ApJ, 237, 692

Leavitt H. S., Pickering E. C., 1912, Harvard College Observatory Circular, 173, 1

Lin L., Patton D. R., Koo C. D., Casteels K., Hsieh B. C., 2008, in Kodama T., Yamada T., Aoki K., eds, Astronomical Society of the Pacific Conference Series Vol. 399, Panoramic Views of Galaxy Formation and Evolution. p. 298

Lin L., et al., 2010, ApJ, 718, 1158

Lintott C. J., et al., 2008, MNRAS, 389, 1179

Lintott C., et al., 2011a, VizieR Online Data Catalog, p. J/MNRAS/410/166

Lintott C., et al., 2011b, MNRAS, 410, 166

Lopes P. A. A., Ribeiro A. L. B., Brambila D., 2024, MNRAS, 527, L19

Lotz J. M., Jonsson P., Cox T. J., Croton D., Primack J. R., Somerville R. S., Stewart K., 2011, ApJ, 742, 103

Madau P., Pozzetti L., Dickinson M., 1998, ApJ, 498, 106

Mahajan S., Mamon G. A., Raychaudhury S., 2011, MNRAS, 416, 2882

Mamon G. A., 2007, in Saviane I., Ivanov V. D., Borissova J., eds, Groups of Galaxies in the Nearby Universe. p. 203 (arXiv:astro-ph/0607482), doi:10.1007/978-3-540-71173-5˙35

Mamon G. A., Sanchis T., Salvador-Solé E., Solanes J. M., 2004, A&A, 414, 445

Martig M., Bournaud F., Teyssier R., Dekel A., 2009, ApJ, 707, 250

Martig M., et al., 2013, MNRAS, 432, 1914

Martin D. C., et al., 2005, ApJ, 619, L1

Martin D. C., et al., 2007, ApJS, 173, 342

Martínez H. J., Coenda V., Muriel H., de los Rios M., Ruiz A. N., 2023, MNRAS, 519, 4360

Masters K. L., et al., 2010, MNRAS, 405, 783

Masters K. L., et al., 2019, MNRAS, 487, 1808

Mastropietro C., Moore B., Mayer L., Debattista V. P., Piffaretti R., Stadel J., 2005, MNRAS, 364, 607

Matzner C. D., 2002, ApJ, 566, 302

McGee S. L., Balogh M. L., Bower R. G., Font A. S., McCarthy I. G., 2009, MNRAS, 400, 937

McKee C. F., Ostriker J. P., 1977, ApJ, 218, 148

McKinney W., et al., 2010, in Proceedings of the 9th Python in Science Conference. pp 56–61, doi:10.25080/Majora-92bf1922-00a

Meert A., Vikram V., Bernardi M., 2015, MNRAS, 446, 3943

Mendel J. T., Simard L., Palmer M., Ellison S. L., Patton D. R., 2014, ApJS, 210, 3

Messier C., 1774, Mémoires de l'Académie Royale des Sciences, VIII (P1), 435

Mirabel I. F., et al., 1998, A&A, 333, L1

Molendi S., 2004, in Bertin G., Farina D., Pozzoli R., eds, American Institute of Physics Conference Series Vol. 703, Plasmas in the Laboratory and in the Universe: New Insights and New Challenges. pp 345–354 (arXiv:astro-ph/0404410), doi:10.1063/1.1718479

Moore B., Katz N., Lake G., Dressler A., Oemler A., 1996, Nature, 379, 613

Moore B., Lake G., Katz N., 1998, ApJ, 495, 139

Moore B., Lake G., Quinn T., Stadel J., 1999, MNRAS, 304, 465

Moustakas J., Kennicutt Robert C. J., Tremonti C. A., 2006, ApJ, 642, 775

Muzzin A., et al., 2014, ApJ, 796, 65

Nair P. B., Abraham R. G., 2010, ApJS, 186, 427

Noeske K. G., et al., 2007, ApJ, 660, L43

Oman K. A., Hudson M. J., 2016, MNRAS, 463, 3083

Oogi T., Habe A., 2013, MNRAS, 428, 641

Park C., Hwang H. S., 2009, ApJ, 699, 1595

Pasquali A., Smith R., Gallazzi A., De Lucia G., Zibetti S., Hirschmann M., Yi S. K., 2019, MNRAS, 484, 1702

Peng C. Y., Ho L. C., Impey C. D., Rix H.-W., 2002, AJ, 124, 266

Peng C. Y., Ho L. C., Impey C. D., Rix H.-W., 2010a, AJ, 139, 2097

Peng Y.-j., et al., 2010b, ApJ, 721, 193

Peng Y., Maiolino R., Cochrane R., 2015, Nature, 521, 192

Petersson J., Renaud F., Agertz O., Dekel A., Duc P.-A., 2023, MNRAS, 518, 3261

Poggianti B. M., et al., 2017, ApJ, 844, 48

Popesso P., et al., 2019, MNRAS, 483, 3213

Popesso P., et al., 2023, MNRAS, 519, 1526

Postman M., et al., 2005, ApJ, 623, 721

Prescott M., et al., 2011, MNRAS, 417, 1374

Press W. H., Davis M., 1982, ApJ, 259, 449

Quilis V., Moore B., Bower R., 2000, Science, 288, 1617

Quilley L., de Lapparent V., 2022, A&A, 666, A170

Rampazzo R., et al., 2007, MNRAS, 381, 245

Rampazzo R., Omizzolo A., Uslenghi M., Román J., Mazzei P., Verdes-Montenegro L., Marino A., Jones M. G., 2020, A&A, 640, A38

Reduzzi L., Longhetti M., Rampazzo R., 1996, MNRAS, 282, 149

Reines A. E., Volonteri M., 2015, ApJ, 813, 82

Rhee J., Smith R., Choi H., Yi S. K., Jaffé Y., Candlish G., Sánchez-Jánssen R., 2017, ApJ, 843, 128

Rhee J., Smith R., Choi H., Contini E., Jung S. L., Han S., Yi S. K., 2020, ApJS, 247, 45

Roberts I. D., Parker L. C., 2017, MNRAS, 467, 3268

Roberts I. D., Parker L. C., 2020, MNRAS, 495, 554

Roberts I. D., Parker L. C., Brown T., Joshi G. D., Hlavacek-Larrondo J., Wadsley J., 2019, ApJ, 873, 42

Roberts I. D., et al., 2022, ApJ, 941, 77

Robotham A. S. G., et al., 2013, MNRAS, 431, 167

Robotham A. S. G., Bellstedt S., Lagos C. d. P., Thorne J. E., Davies L. J., Driver S. P., Bravo M., 2020, MNRAS, 495, 905

Rubin V. C., Ford W. Kent J., 1970, ApJ, 159, 379

Rubin V. C., Ford W. K. J., Thonnard N., 1980, ApJ, 238, 471

Salim S., 2014, Serbian Astronomical Journal, 189, 1

Salim S., et al., 2016, ApJS, 227, 2

Salim S., Boquien M., Lee J. C., 2018, ApJ, 859, 11

Sampaio V. M., de Carvalho R. R., Ferreras I., Aragón-Salamanca A., Parker L. C., 2022, MNRAS, 509, 567

Sanders D. B., Mirabel I. F., 1996, ARA&A, 34, 749

Schawinski K., et al., 2006, Nature, 442, 888

Schawinski K., Thomas D., Sarzi M., Maraston C., Kaviraj S., Joo S.-J., Yi S. K., Silk J., 2007, MNRAS, 382, 1415

Schawinski K., et al., 2014, MNRAS, 440, 889

Scoville N., et al., 2007, ApJS, 172, 1

Sengupta A., Keel W. C., Morrison G., Windhorst R. A., Miller N., Smith B., 2022, ApJS, 258, 32

Sérsic J. L., 1963, Boletin de la Asociacion Argentina de Astronomia La Plata Argentina, 6, 41

Sersic J. L., 1968, Atlas de Galaxias Australes

Shen S., Mo H. J., White S. D. M., Blanton M. R., Kauffmann G., Voges W., Brinkmann J., Csabai I., 2003, MNRAS, 343, 978

Simard L., et al., 2002, ApJS, 142, 1

Simard L., et al., 2009, A&A, 508, 1141

Simard L., Mendel J. T., Patton D. R., Ellison S. L., McConnachie A. W., 2011, ApJS, 196, 11

Smith R., Davies J. I., Nelson A. H., 2010a, MNRAS, 405, 1723

Smith R. J., et al., 2010b, MNRAS, 408, 1417

Somerville R. S., Davé R., 2015, ARA&A, 53, 51

Speagle J. S., Steinhardt C. L., Capak P. L., Silverman J. D., 2014, ApJS, 214, 15

Springel V., et al., 2005, Nature, 435, 629

Strateva I., et al., 2001, AJ, 122, 1861

Su K.-Y., et al., 2019, MNRAS, 487, 4393

Sun M., Donahue M., Voit G. M., 2007, ApJ, 671, 190

Tanaka M., Goto T., Okamura S., Shimasaku K., Brinkmann J., 2004, AJ, 128, 2677

Taylor M. B., 2005, in Shopbell P., Britton M., Ebert R., eds, Astronomical Society of the Pacific Conference Series Vol. 347, Astronomical Data Analysis Software and Systems XIV. p. 29

Taylor E. N., et al., 2023, The Messenger, 190, 46

Tenorio-Tagle G., Bodenheimer P., 1988, ARA&A, 26, 145

Tenorio Tagle G., Yorke H. W., Bodenheimer P., 1979, A&A, 145, 110

Thorne J. E., et al., 2021, MNRAS, 505, 540

Tinsley B. M., 1980, Fund. Cosmic Phys., 5, 287

Tomczak A. R., et al., 2016, ApJ, 817, 118

Tomisaka K., Ikeuchi S., 1986, PASJ, 38, 697

Toomre A., Toomre J., 1972, ApJ, 178, 623

Tran K.-V. H., Simard L., Illingworth G., Franx M., 2003, ApJ, 590, 238

Troncoso-Iribarren P., Padilla N., Santander C., Lagos C. D. P., García-Lambas D., Rodríguez S., Contreras S., 2020, MNRAS, 497, 4145

Trussler J., Maiolino R., Maraston C., Peng Y., Thomas D., Goddard D., Lian J., 2020, MNRAS, 491, 5406

Varela J., Moles M., Márquez I., Galletta G., Masegosa J., Bettoni D., 2004, A&A, 420, 873

Vazdekis A., 1999, ApJ, 513, 224

Vikram V., Wadadekar Y., Kembhavi A. K., Vijayagovindan G. V., 2010, MNRAS, 409, 1379

Virtanen P., et al., 2020, Nature Methods, 17, 261

Vulcani B., et al., 2018, ApJ, 866, L25

Walch S. K., Whitworth A. P., Bisbas T., Wünsch R., Hubber D., 2012, MNRAS, 427, 625

Walcher J., Groves B., Budavári T., Dale D., 2011, Ap&SS, 331, 1

Wang J., et al., 2012, MNRAS, 423, 3486

Wechsler R. H., Tinker J. L., 2018, ARA&A, 56, 435

Werner M. W., et al., 2004, ApJS, 154, 1

Wetzel A. R., Tinker J. L., Conroy C., 2012, MNRAS, 424, 232

Wetzel A. R., Tinker J. L., Conroy C., van den Bosch F. C., 2013, MNRAS, 432, 336

Wetzel A. R., Deason A. J., Garrison-Kimmel S., 2015a, ApJ, 807, 49

Wetzel A. R., Tollerud E. J., Weisz D. R., 2015b, ApJ, 808, L27

White S. D. M., et al., 2005, VizieR Online Data Catalog, pp J/A+A/444/365

Willett K. W., et al., 2013, MNRAS, 435, 2835

Williams J. P., McKee C. F., 1997, ApJ, 476, 166

Wilman D. J., Oemler A. J., Mulchaey J. S., McGee S. L., Balogh M. L., Bower R. G., 2009, ApJ, 692, 298

Woods D. F., Geller M. J., Barton E. J., 2006, AJ, 132, 197

Wright E. L., et al., 2010, AJ, 140, 1868

Yang X., Mo H. J., van den Bosch F. C., Pasquali A., Li C., Barden M., 2007, ApJ, 671, 153

York D. G., et al., 2000, AJ, 120, 1579

Zhang H.-X., Gao Y., Kong X., 2010, MNRAS, 401, 1839

de Carvalho R. R., Djorgovski S., 1992, ApJ, 389, L49

de Vaucouleurs G., 1948, Annales d'Astrophysique, 11, 247

de Vaucouleurs G., 1961, ApJS, 5, 233

de Vaucouleurs G., 1963, ApJS, 8, 31

van den Bosch F. C., Aquino D., Yang X., Mo H. J., Pasquali A., McIntosh D. H., Weinmann S. M., Kang X., 2008, MNRAS, 387, 79